Oligosaccharyltransferase is involved in targeting to ER-associated degradation

Marina Shenkman[1,2], Navit Ogen-Shtern[1,3], Chaitanya Patel[1,2], Bella Groisman[1], Metsada Pasmanik-Chor[4], Sonya M. Schermann[5,6], Roman Körner[5] and Gerardo Z. Lederkremer[1,2,] *

[1]The Shmunis School of Biomedicine and Cancer Research, Cell Biology Division, George Wise Faculty of Life Sciences, Tel Aviv University, Tel Aviv 69978, Israel

[2]Sagol School of Neuroscience, Tel Aviv University, Tel Aviv 69978, Israel

[3]Present address: The Skin Research Institute, The Dead-Sea and Arava Science Centre, Masada 86910, Israel

[4]Bioinformatics Unit, George Wise Faculty of Life Sciences, Tel Aviv University, Tel Aviv 69978, Israel

[5]Max Planck Institute of Biochemistry, Martinsried D-82152, Germany.

[6]Ascend Advanced Therapies, Martinsried, Germany.

* Corresponding author: Gerardo Z. Lederkremer

Email: gerardol@tauex.tau.ac.il

Keywords: endoplasmic reticulum/ ERAD/ HRD1/ OST/ retrotranslocation.

Abstract

Most membrane and secretory proteins undergo N-glycosylation, catalyzed by oligosaccharyltransferase (OST), a membrane-bound complex in the endoplasmic reticulum (ER). Proteins failing quality control are degraded via ER-associated degradation (ERAD), involving retrotranslocation to cytosolic proteasomes. Using SILAC proteomics, we identified OST subunits as key interactors with a misfolded ER protein bait, suggesting unexpected involvement in ERAD. Previous reports implied additional roles for OST subunits beyond N-glycosylation, such as quality control by ribophorin I. We tested OST engagement in glycoprotein and non-glycosylated protein ERAD; overexpression or partial knockdown of OST subunits interfered with ERAD in conditions that did not affect glycosylation. Effects were studied on misfolded membrane proteins, BACE476 and asialoglycoprotein receptor H2a, and the luminal α1-antitrypsin NHK variant. OST appears to participate in late ERAD stages, interacting with the E3 ligase HRD1 and facilitating retrotranslocation. Molecular dynamics simulations suggest membrane thinning by OST transmembrane domains, possibly assisting retrotranslocation via membrane distortion.

Introduction

Secretory proteins are translocated into the endoplasmic reticulum (ER), where they undergo folding and quality control. Molecules that are terminally misfolded are retrotranslocated to the cytosol to be polyubiquitinated and degraded by proteasomes, in a process known as ER-associated degradation (ERAD) [1,2]. The precise mechanism of retrotranslocation remains a subject of ongoing study. It appears that various mechanisms may exist for different ERAD substrates, contingent upon the specific E3 ubiquitin ligase involved. Among these ligases, the most well-characterized participant in ERAD is HRD1, which forms a large protein complex mediating retrotranslocation [3,4]. Studies using genetic screens in yeast identified ERAD complexes involving HRD1 [5]. Subsequently, analogous components were found in mammals, including HRD1 itself [6]. The primary constituents of the mammalian HRD1 complex encompass transmembrane proteins such as Derlin 1-3, Herp, and Ubxd8, along with SEL1L, OS9, and XTP3-B on the luminal side. On the cytosolic side, components include Ubc6 or Ube2G2, p97, and NGLY1 [3,5]. Structural insight into the HRD1 complex has been reported in yeast but not yet in mammalian cells [7,8]. Cryo-electron microscopy (CryoEM) studies of the yeast HRD1/HRD3 complex indicated a direct role in retrotranslocation [7]. Further evidence involves *in vitro* reconstitution experiments suggesting a regulation of retrotranslocation by HRD1 autoubiquitination [9,10]. Herp, a protein tethered to the ER membrane via a hydrophobic hairpin, with most of the protein on the cytosolic side, was shown to recruit HRD1 and misfolded proteins for ERAD at a specialized ER subcompartment, the ERQC [11,12].

An approach used to delineate the HRD1 complex and discover new components has been the pull-down of the complex through known ERAD components, such as Yos9 in yeast [13] and SEL1L [14], XTP-3B, HRD1, UBXD8, Derlin-1/2 and OS-9 in mammalian cells [15]. The caveat is that overexpression affects the function and interactions of these proteins. Furthermore, even when tagged by knock-in at the endogenous level the isolated complexes might be non-functional [16]. This is because these complexes might be dormant, partial complexes, given the dynamic nature of complex assembly, influenced by the presence of an ERAD substrate [11,17]. Here we have used a SILAC (stable isotope labeling by amino acids in cell culture) proteomics approach to capture functional ERAD components. We accomplish this by pull-down of an ERAD substrate and analyzing its preferential interactors under conditions favoring the accumulation of molecules targeted for retrotranslocation and subsequent proteasomal degradation. Surprisingly, among the most highly enriched interactors were several subunits of the oligosaccharyltransferase (OST) complex.

OST plays a pivotal role in N-glycosylation, the primary post-translational modification of secretory proteins. It transfers a conserved oligosaccharide from a lipid-linked glycan donor to asparagine residues in defined sequons in newly-synthesized proteins. In mammalian cells, the OST complex consists of a catalytic transmembrane subunit (STT3A or STT3B) along with

several additional transmembrane proteins including DAD1, OST48/DDOST, TMEM258, OST4, ribophorin1, ribophorin2, and subunits interacting with STT3A (KCP2, DC2/OSTC) or STT3B (TUSC3/N33 or IAP/MAGT1) [18,19]. While the primary function of the OST complex lies in protein N-glycosylation, studies suggest the participation of OST subunits, such as ribophorin I, in protein quality control [20,21], although the mode of action remains unclear. Here we show that OST subunits have a role in protein targeting to ERAD.

Results

Identification of OST as ERAD substrate interactor by a SILAC proteomics approach.

The proteomics approach that we devised involved making a construct of an established model ERAD substrate, H2a, with an affinity binding tag (streptavidin binding peptide, SBP) and producing a stable HEK293 cell line (SBP6) expressing this fusion protein, H2aSBP. H2a, the uncleaved precursor of human asialoglycoprotein receptor (ASGPR) H2a, has been extensively studied. H2a is a type II membrane glycoprotein, completely retained in the ER [22] and is a substrate of the HRD1 complex [11,23]. As H2a can undergo natural cleavage, generating a soluble luminal fragment, we used an uncleavable mutant, H2aG78R [24]. The use of the 38 amino acid SBP affinity tag allows for specific and high affinity binding and elution under mild conditions, to preserve complexes [25]. H2aSBP behaves like H2a in its ER retention and targeting to ERAD and H2aSBP precipitation with streptavidin beads allows coprecipitation of Derlin1, HRD1 and Fbs2, with the latter interaction being inhibited with kifunensin, which inhibits mannose trimming required for ERAD [23].

SBP6 cells were cultured in the presence of media containing heavy amino acids (13C(6)15N(2) lysine) to uniformly label the proteins, while WT HEK293 cells were grown with normal light amino acids, or vice versa (Fig. 1a). Cell lysates in mild non-denaturing detergent (1% digitonin) from cells with or without H2aSBP expression were mixed at a 1:1 protein ratio, followed by precipitation with streptavidin-conjugated beads and elution by competition with biotin. Eluted proteins were subjected to SDS-PAGE, digested with trypsin and identified by electrospray tandem mass spectrometry (ESI-MS/MS). This experiment was done in cells treated without or with proteasomal inhibitors to accumulate the ERAD substrate before degradation. Both cells treated with or without proteasomal inhibitors were incubated briefly with puromycin before cell lysis, to reduce the amount of proteins undergoing cotranslational translocation into the ER. Puromycin causes the termination of nascent polypeptide chains and their release into the lumen of the ER [26].

The expression of H2aSBP increased by proteasomal inhibition and more robustly by overexpression of a dominant negative RING finger mutant of HRD1, as expected for an HRD1 substrate. The mutant HRD1 coprecipitated with H2aSBP upon pull-down of the latter with streptavidin-agarose beads (Fig. 1b).

The SBP tag allowed specific and efficient elution in non-denaturing conditions with a competitive concentration of free biotin, showing many proteins coprecipitated specifically from a lysate of cells labeled with [^{35}S] met+cys in the presence of the proteasome inhibitor MG-132 (Fig. 1c). Brief treatment with puromycin before lysis did not decrease the signal of these proteins. We used mild lysis conditions (see Methods), combined with the gentle biotin elution, to enable preservation of protein complexes with little or no non-specific precipitation. Silver staining of the eluates after SDS-PAGE in a similar experiment showed an excellent signal to noise ratio, with only very weak bands in the control without H2aSBP, except for BSA, which was used as a blocker to reduce non-specific binding during the affinity pull-down. (Fig. 1d).

After applying the SILAC proteomics protocol (Fig. 1a), we selected as interactors only hits showing >2 fold ratio of labeled/ unlabeled after normalization to the total amount of H2a-SBP (bait) obtained. We then compared the results from cells treated for 4h with MG-132 and ALLN and 15 min with puromycin to those from cells treated only with puromycin. Gene ontology analysis showed that proteasomal inhibition led to a significant enrichment for cellular functions related to the ER, ER membrane and ubiquitin/proteasome processes, which were expected, and gave us confidence in the approach. One of the top function enriched categories using the DAVID gene enrichment tool was the OST complex (p-value=$3.13e^{-10}$), which was unexpected (Fig. 1e). A STRING interaction map showed high enrichment of proteins belonging to a few categories related to protein

quality control: ERAD (p-value=1.28e^{-7}), protein folding (p-value=1.28e^{-7}), glycosylation (p-value=7.03e^{-10})(including OST and calnexin (CNX) cycle genes), unfolded protein response (UPR) and vesicular transport (p-value=8.00e^{-6})(Fig. 1f). This latter category perhaps relates to the participation of vesicular trafficking in ERAD, which we reported recently [27].

Among the most significant H2aSBP interactors, with enrichment values of 2-fold or higher in proteasomal inhibitor-treated cells, were most OST subunits (Table 1). This was even more surprising, considering that membrane proteins, some with multiple membrane spans such as OST subunits, are usually underrepresented in the MS analysis. All of these OST subunits were highly enriched upon proteasomal inhibition (Fig. 1g). It should be stressed that the puromycin treatment before cell lysis should have reduced interactions with newly-made translocated proteins, where H2aSBP could have encountered OST, which is associated with forward translocons [28]. Indeed, levels of forward translocon related proteins, such as Sec61 subunits or SSRA were at similar or reduced levels in samples treated with or without proteasomal inhibitor (Fig. 1g). Other enriched proteins in proteasomal inhibitor-treated samples include ERAD-related genes, such as XTP3-B, SEL1 and ubiquitin, calnexin cycle genes (CNX, SEP15 and UGGT1) and other relevant genes such as the ER calcium pump SERCA2 and TDP43 (Fig. 1g). TDP43, normally localized in the nucleus, accumulates in the cytoplasm in several diseases, including ALS, and also upon proteasome inhibition [29].

Colocalization and increased interaction of an OST subunit with the ERAD substrate upon proteasomal inhibition.

Given the increase in the pull-down of OST subunits with the ERAD substrate upon proteasomal inhibition, we then analyzed whether there was any change in the subcellular localization of an OST subunit in relation to the ERAD substrate under these conditions. We chose to examine the OST subunit Defender Against apoptotic cell Death 1 (DAD1) [30] because it was well characterized in previous studies, although it was not detected in our proteomics analysis, possibly due to its low abundance. GFP-DAD1 had been shown to associate with forward translocons [31]. We compared the localization of GFP-DAD1 to the ERAD substrate H2a linked to monomeric red fluorescent protein (H2a-RFP). Both GFP-DAD1 and H2a-RFP show an ER pattern in untreated cells, although with some concentration in the juxtanuclear region (Fig. 2a). Surprisingly, under proteasomal inhibition with lactacystin (Lac), GFP-DAD1 accumulated together with H2a-RFP in the juxtanuclear ER-derived quality control compartment (ERQC), a staging ground for ERAD [12,24,32], (Fig. 2b). This is similar to the effect of ERAD substrate accumulation (upon proteasomal inhibition or by other means) on the localization of ERAD machinery components (HRD1, Derlin-1 [23]). Several ER chaperones, such as CNX and CRT, also relocalize to the ERQC under these conditions, but not others, such as BiP [32,33]. As we had also seen before [24], the translocon subunit Sec61β linked to GFP accumulates at the ERQC with the ERAD substrate upon proteasomal inhibition (Fig. 2c, d). To test whether the entire translocation complex linked to ribosomes (at the rough ER) accumulates in the ERQC along with the ERAD substrate, we immunostained cells transfected with H2a-RFP using an anti-ribosomal RNA (rRNA) antibody as a ribosomal marker. As opposed to DAD1 and Sec61β, the ribosomes did not accumulate together with H2a-RFP after Lac treatment and remained in a cytosolic and ER pattern (Fig. 2e, f). Sec61 participates in the forward translocation complex, but has also been implicated in retrotranslocation [34].

We compared the localization of GFP-DAD1 with that of the ERAD-associated luminal lectin OS-9, which appears constitutively localized mainly at the ERQC [11,35]. Similar to H2a-RFP, the GFP-DAD1 that accumulated under proteasomal inhibition colocalized with OS-9 (Fig. 2 h, k). In this experiment bortezomib (Bz) was used for proteasome inhibition. However, while the colocalization of H2a-RFP with OS-9 increased significantly upon proteasomal inhibition, that of GFP-DAD1 did not change (Fig. 2 i, l). This suggests that a portion of GFP-DAD1 molecules localize to the ERQC in untreated cells and may already colocalize with OS-9 in peripheral regions.

We used iodixanol gradients optimized to separate ER subcompartments as a different approach to analyze the localization of these proteins in relation to the ERQC [11,36]. As we had seen before [11], H2a-RFP appeared mainly in middle fractions of the gradient (5-7), with a small shift to heavier fractions (6-8), upon proteasomal inhibition with Bz (Fig. 2m). Endogenous DAD1 showed a similar pattern in untreated cells, with a sharper accumulation in Bz-treated cells, as a peak in fraction 6,

192 and an additional smaller peak in fraction 4. Endogenous CNX and Sec61β also appeared in middle
193 fractions, partially overlapping with DAD1 in untreated conditions and in Bz-treated cells where they
194 concentrated in fraction 6. We analyzed another OST subunit, Tumor suppressor candidate 3
195 (Tusc3), a non-essential subunit that was also absent from our top proteomic hits. Endogenous
196 Tusc3 showed a similar pattern to DAD1 in untreated conditions, although concentrating more at
197 fraction 4, but it did not shift to higher densities upon proteasomal inhibition (Fig. 2m). A ribosomal
198 subunit, RPL26 appeared at higher densities, marking regions of rough ER, with little or no overlap
199 with the ERQC (Fig. 2m), as we had seen before [11].
200 A specific interaction of GFP-DAD1 and H2a was detected by coimmunoprecipitation (Fig. 2n),
201 which was significantly increased upon proteasomal inhibition, suggesting that molecules targeted
202 for degradation have a higher probability of interacting than newly made ones.
203 In summary, upon proteasomal inhibition DAD1 accumulates in the ERQC, in association with an
204 ERAD substrate and separate from the rough ER, which contains forward translocons.
205
206 **OST subunits promote the degradation of glycosylated H2a and to a lesser extent of its non-**
207 **glycosylated mutant**
208 To investigate a possible role of OST in ERAD, we first overexpressed GFP-DAD1 and analyzed
209 its effect on H2a. Overexpression of GFP-DAD1 led to a dramatic decrease in the levels of H2a
210 (Fig. 3a), suggesting that the protein was degraded. There was no change in the migration of H2a,
211 indicating that glycosylation was not affected. We then partially knocked down DAD1 (Suppl. Fig.
212 1), which had a major effect in increasing the levels of H2a, suggesting that ERAD was inhibited
213 (Fig. 3b). This partial knockdown had only a very minor effect on glycosylation, as a weak band of
214 faster migration appeared suggesting the existence of a small population of underglycosylated
215 molecules (2 of the 3 glycosylation sites occupied according to our previous studies [37]). We then
216 tried partially knocking down Tusc3 (Suppl. Fig. 1), which also caused a major accumulation of H2a
217 (Fig. 3c). Tusc3 is a non-essential OST subunit, but nevertheless also caused the appearance of
218 a minor population of underglycosylated H2a molecules. Therefore, partial knockdown of DAD1 or
219 Tusc3, in conditions that affect minimally OST function in glycosylation, have a major effect on
220 inhibiting ERAD.
221 To confirm that the effects on the steady state levels of H2a were due to changes in its degradation,
222 we performed pulse-chase analysis experiments using [^{35}S] cys metabolic labeling. The
223 overexpression of GFP-DAD1 led to a significantly accelerated degradation of H2a (Fig. 3d).
224 Conversely, knockdown of Tusc3 strongly slowed down the degradation (Fig. 3e).
225 Although glycosylation of H2a did not seem to be affected, we wanted to test whether the effect of
226 Tusc3 knockdown on H2a degradation could be due to inhibition of N-glycosylation of key
227 components of quality control or ERAD. To test this, we inhibited completely N-glycosylation by a
228 long (18h) incubation of cells with tunicamycin (Tun), after which we performed a pulse-chase
229 experiment in the presence of Tun. The treatment caused a shift in the migration of H2a due to lack
230 of its 3 N-glycan chains (Fig 3f). However, the rate of H2a degradation showed no significant
231 change in the presence of Tun (Fig 3f graph), which suggests that the effect of Tusc3 knockdown
232 in delaying degradation (Fig. 3c and 3e) cannot be ascribed to inhibition of glycosylation of the
233 ERAD substrate or of ERAD components.
234 Similar experiments were performed on a non-glycosylated mutant of H2a (H2aΔgly, [37]). GFP-
235 DAD1 overexpression and Tusc3 knockdown had similar effects on H2aΔgly as on glycosylated
236 H2a, but to a much lesser extent (compare Fig. 4 a, c, d with Fig. 3 a, c, e respectively). DAD1
237 knockdown did not have any effect on H2aΔgly degradation (Fig. 4b). DAD1 does not seem to
238 participate in H2aΔgly ERAD at its endogenous levels, but can target the non-glycosylated protein
239 when DAD1 is overexpressed.
240
241 **OST subunits participate in ERAD of other membrane and luminal substrates**
242 To test whether OST subunits are more generally involved in ERAD, we analyzed other well-
243 established ERAD substrates, BACE476, a mutant type I membrane-bound glycoprotein (in
244 contrast with H2a, which is type II, [11]) and the soluble luminal misfolded glycoprotein human α1-
245 antitrypsin variant null Hong Kong (NHK) [38]. Overexpression of GFP-DAD1 led to a decrease in the
246 levels of BACE476 and NHK, although to a much lesser extent than for H2a (compare Fig. 5 a, d

247 to Fig. 3a). Similarly, DAD1 or Tusc3 knockdown caused an accumulation of BACE476 and NHK
248 but again less pronounced than for H2a (compare Fig. 5 b, c, e, f to Fig. 3 b,c).
249 Thus, OST subunits can promote ERAD of type I or type II transmembrane substrates and of a
250 soluble luminal substrate, but with some differences in the extent of their action depending on the
251 substrate.
252
253 **Interaction between DAD1 and HRD1 and promotion of retrotranslocation by OST subunits**
254 As the ERAD substrates used in our experiments are targeted to HRD1, we wondered whether
255 DAD1 and HRD1 interact. In a coimmunoprecipitation experiment, we could see a robust and
256 specific interaction between GFP-DAD1 and HRD1-myc (Fig. 6a). Although both DAD1 and HRD1
257 accumulated upon proteasomal inhibition, the ratio of DAD1 coimmunoprecipitated in association
258 with HRD1 decreased (Fig. 6a graph). This suggests that possibly DAD1 associates with HRD1 in
259 a functional ER membrane complex and does not interact with HRD1 molecules that are already
260 targeted for proteasomal degradation.
261 We next studied the requirement of OST subunits for the retrotranslocation step. We tested the
262 effect of manipulating the levels of OST subunits on retrotranslocation using the BAP/BirA system
263 [39]. This system utilizes the E. coli biotin ligase BirA expressed in the cytosol of mammalian cells to
264 specifically biotinylate a 15 amino acid biotin-acceptor peptide (BAP). Secretory proteins with a
265 BAP tag on their ER luminal side are biotinylated only after retrotranslocation. A construct of H2a
266 with BAP attached to its luminal C-terminus behaved consistently as expected for a type II
267 membrane protein [40]. H2a-BAP was biotinylated poorly when coexpressed with cytosolic BirA, but
268 to a much higher extent when coexpressed with a luminally expressed secBirA, which contains a
269 signal peptide for translocation into the ER [39] (Fig. 6b). There was no biotinylation in a control
270 without BirA or secBirA. As BAP is on the luminal C-terminus of H2a, it can be exposed to the
271 cytosolic BirA only after H2a-BAP retrotranslocation. Overexposure of the cytosolic biotinylated
272 retrotranslocated H2a signal allowed us to assess the effect of overexpression or knockdown of
273 OST subunits (Fig. 6c). GFP-DAD1 overexpression caused a decrease in total H2aBAP, as
274 observed for H2a (Fig. 6c lower panel, compared to Fig. 3a), but there was a much smaller
275 decrease in retrotranslocated biotinylated H2aBAP (Fig. 6c upper panel), resulting in a large
276 increase in the ratio of retrotranslocated molecules relative to total, as compared to the control (Fig.
277 6c graph). Knockdown of either DAD1 or Tusc3 had the opposite effect, resulting in a significant
278 decrease in the retrotranslocation ratio compared to the control.
279 Together, these results suggest that OST interacts with HRD1 and participates in the
280 retrotranslocation process towards ERAD.
281
282 **Molecular dynamics simulation suggest membrane thinning by OST**
283 The molecular architecture of the human OST complexes had been determined by cryo-EM [41],
284 showing a dense region traversing the ER membrane with multiple transmembrane domains. (Fig.
285 7 a,b). Molecular dynamics simulations (pre-rendered at the MemProtMD database [42]) indicate
286 substantial membrane thinning by the OST transmembrane domains (Fig. 7 c,d). This may lower
287 the energy barrier for protein retrotranslocation, or dislocation from the membrane, as proposed for
288 the interphase between HRD1 and Der1 in yeast [43].
289
290
291 **Discussion**
292
293 In the present study we aimed to identify ERAD machinery components through their interaction
294 with a model misfolded protein being targeted to this pathway. For this aim, we developed an
295 approach for isolation of functional protein complexes engaged in the retrotranslocation event,
296 under conditions in which there is enrichment in retrotranslocation complexes, while minimizing the
297 abundance of forward translocons. This approach employed proteasomal inhibition to accumulate
298 the ERAD substrate just prior to degradation. Our previous studies with H2a, the model substrate
299 used, indicated that in these conditions H2a accumulates in the ERQC membrane, because its
300 retrotranslocation appears to be coupled to its degradation [11,12,24,32]. To reduce the presence of
301 components of the forward translocon in the protein complexes obtained, we incubated the cells

302 with puromycin. This antibiotic causes release of nascent chains from the ribosome and as a result
303 from the translocons. The combination of puromycin treatment with the C-terminal SBP tag used
304 as bait was intended to prevent isolation of the machineries in charge of translation and forward
305 translocation through incompletely translated H2aSBP molecules (which would lack a complete
306 SBP). In these conditions, we observed an association of several of the OST subunits along with
307 H2a in pulldown experiments. Notably, some of these subunits, OSTC, STT3A and MAGT1 were
308 detected only after proteasome inhibition (Fig. 1g); this, together with the puromycin treatment
309 suggests a preferential interaction with the ERAD substrate after its translation and translocation.
310 Consistently, coimmunoprecipitation of DAD1 occurred after full glycosylation of H2a (Fig. 2n).
311 OST association was reported with other ER proteins in different high MW complexes, one of them
312 containing SSRD (Trap delta) [44]. Interestingly, we also detected SSRD only after puromycin
313 treatment and proteasome inhibition (Fig. 1g). Mutations in SSRD lead to defects in glycosylation
314 [45], suggesting an early cotranslational event, as the SSR/ Trap complex has been implicated in
315 forward translocation. However, an alternative role has also been suggested for this complex in
316 ERAD [46,47]. Other ER proteins have been suggested to participate in both forward translocation and
317 in retrotranslocation towards ERAD, such as calumin (CCDC47) [48], and the Sec61 complex, for
318 which interaction was found with ERAD factors [34]. Consistently, we found Sec61 subunits and
319 CCDC47 at similar levels in cells with and without proteasomal inhibition (Fig. 1g). It is noteworthy
320 that TDP-43 appeared enriched in cells with proteasomal inhibition. TDP-43 is localized mainly in
321 the nucleus but has been found sequestered at the cytosolic face of the ER in ALS [49].
322 For OST, noncanonical activities have also been suggested, such as that required for Dengue virus
323 infection, which could be sustained with catalytically inactive OST subunits [50]. The OST subunit
324 MAGT1 and its oxidoreductase activity [51] appeared essential for the infection. MAGT1 was present
325 as one of the most significant interactors of our substrate under proteasome inhibition (Fig. 1g).
326 MAGT1 is found associated with an STT3B containing complex [52]. The presence of MAGT1 and
327 the effects of knockdown of Tusc3 (also associated with STT3B) would implicate the STT3B
328 complex in our study. STT3B was not detected in the proteomics results, perhaps due to low
329 abundancy, but STT3A and its associated OSTC were, suggesting also a participation of the
330 STT3A complex in ERAD (Fig. 1g).
331 There are previous studies that hint to the participation of OST subunits in quality control and
332 ERAD. It was suggested that ribophorin I might be involved in protein quality control, as it interacted
333 with a quality control substrate, a fragment of the amyloid precursor protein, after its translocation,
334 remaining associated after puromycin release [21]. In the case of ERAD highjacking by CMV, the
335 CMV US11 protein was found associated with OST subunits, ribophorin 1, ribophorin 2, and OST48
336 [53]. The ER protein malectin forms a complex with ribophorin 1 which retains misfolded NHK α1-
337 antitrypsin and misfolded ribonuclease A but not the WT counterparts in the ER [20]. In a proteomics
338 study using OS-9 as a bait, Christianson et al pulled down ribophorin 1 with high score [54]. They
339 also pulled down other OST subunits, such as STT3A, STT3B and DAD1 using UbxD8, Derlin-1 or
340 Derlin-2 as baits [15]. However, these observations were not further investigated.
341 Our proteomics findings, along with insights from the effects of modulating DAD1 and Tusc3 levels,
342 strongly suggest the participation of most, if not all, OST subunits in ERAD. It is likely that DAD1
343 and Tusc3 fell below the detection threshold in our proteomics analysis. Despite this, DAD1
344 exhibited clear associations with the ERAD substrate (Fig. 2n) and HRD1 (Fig. 6a) and showed
345 strong effects of its overexpression. The effect of overexpression of this single OST subunit on
346 ERAD might be explained by the limited quantity of its endogenous expression in relation to other
347 subunits [55]. Interestingly, both DAD1 and Tusc3 partial knockdowns significantly affected ERAD
348 without any significant change in glycosylation.
349 Both DAD1 and Sec61β relocalized to the ERQC under proteasomal inhibition (Fig. 2), suggesting
350 that most of their molecules are associated with the ERQC and not with forward translocons in
351 these conditions. In a previous study, GFP-DAD1 had been observed to remain with relatively low
352 mobility in the ER membrane, even after puromycin termination of protein synthesis and release
353 from translocons. This observation led to the conclusion that GFP-DAD1 probably remains
354 associated with inactive translocons [31]. However, the low mobility after puromycin treatment (as we
355 do here) might instead signify a population of GFP-DAD1 molecules associated with a
356 retrotranslocation complex. Indeed, GFP-DAD1 associates with HRD1 (Fig. 6a). Intriguingly, other

OST subunits were reported to undergo cleavage by the intramembrane rhomboid protease RHBDL4 before being targeted to ERAD [56]. Thus, if GFP-DAD1 were undergoing a similar targeting for ERAD, we would expect to observe cleaved molecules upon association with HRD1, but this was not the case.

In conclusion, OST appears to have a dual role, of N-glycosylation at the initial stages of protein translocation into the ER and aiding ERAD at the final stages in the life of misfolded molecules (Fig. 7e). We can only speculate, with the data that we have at the moment, about how OST precisely contributes to ERAD. The fact that the OST complex encompasses many transmembrane domains, interacts with HRD1, affects retrotranslocation and is predicted to cause membrane thinning suggests that it may participate directly in the mechanism of retrotranslocation. It might contribute to membrane distortion, directly aiding retrotranslocation, similarly to the mechanism proposed for the interphase between HRD1 and Der1 in yeast [43].

Targeting to ERAD has been best studied for glycoproteins and is linked to glycan processing and recognition steps [12]. OST could be a candidate for glycan recognition and targeting to ERAD. However, OST function for ERAD does not appear to be restricted to glycoproteins, although the results of OST subunit overexpression and knockdown suggest some preference for glycosylated substrates (Fig. 3, 4). This dual targeting could be equated to the activities of OS-9, XTP3-B and EDEM1 in targeting both glycoproteins and non-glycoproteins to ERAD [37,57,58].

Materials and Methods

Materials

Streptavidin-agarose-beads, Biotin, tunicamycin, puromycin, MG-132, ALLN, bortezomib, digitonin were from Sigma. Lactacystin was from Cayman Chemicals (Ann Arbor, MI). Promix cell labeling mix ([35S]Met plus [35S]Cys), 1000 Ci/mmol, was from PerkinElmer Life Sciences. Predesigned shRNAs for Tusc3 (TRCN0000038065, TRCN0000038067, TRCN0000299038, TRCN0000299109, TRCN0000299107) and DAD1 (TRCN0000310240, TRCN0000200464, TRCN0000083039, TRCN0000200404, TRCN0000083041) were from Sigma.

Antibodies

Rabbit anti-DAD1, anti-Tusc3 and anti-calnexin, and mouse anti-β tubulin and anti-actin were from Sigma. Mouse anti-HA was from Biolegend and anti-Myc was custom produced and used before [35]. Mouse anti-rRNA from Abcam was a kind gift of Orna Elroy-Stein. Rabbit anti-RPL26 was from Cell Signaling. Rabbit polyclonal anti-H2a carboxy-terminal and amino-terminal antibodies and mouse monoclonal anti–H2a carboxy-terminal antibody B9 were the ones used in earlier studies [11,59]. Mouse anti–S-tag was from Novagen (Gibbstown, NJ). Rabbit anti-GFP was from Santa Cruz Biotech. Rabbit anti-RFP was from MBL. Rabbit anti-Sec61β was the one used previously [32]. Strep-HRP, goat anti-mouse IgG-HRP, goat anti-rabbit IgG-HRP and goat anti-mouse IgG conjugated to Cy2 or to Dylight 549 were from Jackson-Immuno-Research Labs.

Plasmids and constructs

WT HRD1-myc, dominant negative mutant hsHRD1-myc (MutHRD1-myc), Sec61β-GFP, S-tagged-OS-9.1 and S-tagged-OS-9.2 in pcDNA3.1(+), H2a and H2a mutated in its three glycosylation sites (H2aΔgly), subcloned in pCDNA1 and BACE476-HA were used before [11,24,36,60], as well as human α1-antitrypsin NHK-HA in pcDNA3.1 [27]. Constructs encoding H2aG78R uncleavable mutant fused through its C-terminus to a 38-amino acid streptavidin binding peptide (H2aSBP), to monomeric red fluorescent protein (H2aRFP) or to GFP (H2aGFP) were described before [11,23,24]. DAD1 in pEGFP-C1 (GFP- DAD1) was a kind gift from Gert Kreibich. H2a-BAP-V5 was used before [40]. BirA and Sec-BirA plasmids were a kind gift of Gianlucca Petris and Oscar Burrone (ICGEB, Trieste, Italy) [39].

Cell culture, media and transfections

NIH 3T3 and HEK293 cells were grown in DMEM supplemented with 10% bovine calf serum at 37 °C under 5% CO_2. Transfections of NIH 3T3 cells were carried out using a Neon MP-100

412 microporator system (Life Technologies, Carlsbad, CA). Transfection of HEK293 cells was
413 performed using the calcium phosphate method. An HEK293 stable cell line expressing H2aSBP
414 (SBP6) was described previously [23].
415
416 **BAP construct transfection and probing**
417 H2a-BAP-V5 was transfected using the calcium phosphate method in HEK293 cells together with
418 an equal amount of plasmid carrying BirA (cytosolic biotin ligase). Biotin (100μM) was added 24
419 hours post transfection overnight. The cells were then rinsed with PBS and lysed at 4˚C in Buffer
420 A (1% Triton X-100, 0.5% NaDOC and 1X cOmplete Protease Inhibitor Cocktail (Roche) in PBS),
421 containing 10mM N-ethylmaleimide, to block BirA post-lysis activity. The probing of biotinylated
422 proteins on blots was performed using Strep-HRP in PBS-TWEEN (0.5%), followed with detection
423 by enhanced chemiluminescence (ECL).
424
425 **Metabolic labeling**
426 Subconfluent (90%) cell monolayers in 60-mm dishes were labeled for 30 min with [^{35}S]Cys and
427 chased for different periods of time with normal DMEM plus 10% FCS, lysed, and
428 immunoprecipitated with anti-H2a carboxy-terminal antibody as described previously [59,60].
429 Quantitation was performed in a Fujifilm FLA 5100 phosphorimager (Tokyo, Japan).
430
431 **Immunoprecipitation, crosslinking and immunoblotting**
432 Cell lysis in buffer A and immunoprecipitation methods are described in [23]. For GFP-DAD1 co-
433 expressed with H2a, crosslinking was performed with DSP prior to cell lysis. Cells were washed 2X
434 with PBS and incubated with PBS containing 1mM DSP at 4˚C for 1 hour. The reaction was stopped
435 by incubation at 4˚C for 20 min with 50mM Glycine, followed by a rinse with PBS and incubation
436 with 20mM Tris-HCl pH7.4 in PBS for at RT 5 min.
437 For precipitation with streptavidin-agarose beads, cell lysates were incubated with the beads on a
438 vertical rotating mixer at 4°C overnight. After centrifugation, the beads were washed three times
439 with 0.5% Triton X-100, 0.25% NaDOC and 0.5% SDS in PBS and once with PBS. Samples were
440 boiled in sample buffer for 5 minutes and run on SDS-PAGE under reducing conditions.
441 Transfer to a nitrocellulose membrane, immunoblotting, detection by ECL, and quantitation in a
442 Bio-Rad ChemiDocXRS Imaging System (Hercules, CA) were done as described previously [35].
443 Quantity one or ImageJ software were used for the quantitation.
444
445 **Iodixanol equilibrium sedimentation gradient**
446 Iodixanol gradients were performed similarly to previously described [27]. Briefly, HEK293 cells
447 expressing H2a-RFP (untreated or treated with Bz) were washed with PBS, resuspended in a
448 homogenization buffer (0.25M Sucrose, and 10mM HEPES pH7.4). The cells were passed through
449 a 21G needle 5 times before homogenization in a Dounce homogenizer (low clearance pestle, 30
450 strokes). The homogenates were centrifuged at 1000xg for 10 minutes at 4˚C to remove nuclei and
451 cell debris and the supernatants were loaded on top of an iodixanol gradient (10 to 34%). The
452 gradients were ultra-centrifuged at 24,000 rpm (98,500g, Beckman SW41 rotor) at 4˚C for 16 hours.
453 1ml gradient fractions were collected from top to bottom, precipitated with 10% TCA and run on
454 SDS-PAGE.
455
456 **Immunofluorescence Microscopy**
457 Immunofluorescence was performed as described previously [32,61,62]. Briefly, cells grown for 24 h
458 after transfection on coverslips in 24-well plates were fixed with 3% paraformaldehyde for 30 min,
459 incubated with 50mM glycine in PBS, and permeabilized with 0.5% Triton X-100. After blocking
460 with normal goat IgG in PBS/ 2% BSA, they were exposed to primary antibody for 60 min, washed
461 and incubated for 30 min with a secondary antibody, followed by washes and staining of nuclei with
462 DAPI. Specimens were observed on a Zeiss laser scanning confocal microscope (LSM 510; Carl
463 Zeiss, Jena, Germany). ImageJ was used to quantify fluorescence intensity and to calculate
464 Mander's coefficients (using JACOP) for colocalization studies. ERQC localization was determined
465 by the accumulation of H2a fluorescent fusion proteins or of OS-9.
466

467 **Proteomics**
468 SBP binding and elution conditions were as in [63]). For SILAC proteomics HEK293 or SBP6 cells
469 were labeled with 13C(6)15N(2) L-lysine for 10 days. The labeling efficiency obtained was 97%.
470 $7x10^8$ cells (15x150mm dishes) were treated with or without 50μM MG-132 + 50μM ALLN for 4h
471 and with 2mM puromycin for the last 15min before lysis. Cells were lysed in 1% digitonin in
472 PBS+2mM PMSF+5μg/ml aprotinin. Labeled HEK293 and unlabeled SBP6 lysates were mixed at
473 a 1:1 protein ratio. The combined lysates were subjected to ON precipitation with preblocked
474 streptavidin beads (0.5% BSA, 0.2% digitonin in PBS for 2-3 h, washed once with 0.1% BSA in the
475 same buffer composition). Precipitation was with beads in 0.1% BSA, 0.2% digitonin in PBS,
476 followed by 4 washes with 0.2% digitonin in PBS and protein interactors pulled down with H2aSBP
477 were eluted for 1h at +4°C by competition with 250μM free biotin dissolved in the wash buffer.
478 Samples were heated at 65°C with β-mercapto-ethanol containing sample buffer for 10min and run
479 on SDS-PAGE. Proteins were identified by nano LC-MS/MS using a nanoACQUITY UPLC nano
480 liquid chromatography system (Waters) coupled to a LTQ orbitrap mass spectrometer (Thermo) or
481 an EasyLC system (Proxeon) coupled to a Thermo LTQ-FT Ultra mass spectrometer. For nanoLC
482 peptide separation, 15 cm long capillary column (75 μm inner diameter) with a prepulled capillary
483 tip (Proxeon) were packed in-house with Reprosil-Pur 3 μm C18 material (Dr. Maisch). Peptides
484 were eluted at 0.3 μl/min using stepwise gradients from 2%–60% acetonitrile, in 0.1% formic acid.
485 MS/MS analysis on the LTQ orbitrap mass spectrometer was performed with standard settings
486 using cycles of 1 high resolution MS scan from m/z 370-1750 followed by MS/MS scans of the 10
487 most intense ions with charge states of 2 or higher. For analysis on the Thermo LTQ-FT Ultra mass
488 spectrometer, FT scans from m/z 400-2000 were taken at 100,000 resolution, followed by collision
489 induced dissociation (CID) scans in the LTQ of the 8 most intense ions with signal greater than
490 2000 counts, and charge state of 2 or higher.
491
492 **Bioinformatics analysis**
493 Protein identification and SILAC based quantitation was performed with MaxQuant (version
494 1.0.13.13) using default settings. The UNIPROT human database (version 2009-04-14) was used
495 for protein identification. MaxQuant uses a decoy version of the specified UNIPROT database to
496 adjust the false discovery rates for proteins and peptides to below 1%.
497 Gene ontology enrichment of 86 differentially expressed proteins was performed using DAVID tool
498 [64]. Selected enriched functions were presented. Differentially expressed proteins were applied to
499 STRING protein-interaction tool [65]. Protein colors represent enriched functions circled in colors.
500
501 **Statistical Analysis**
502 The results are expressed as average ± SD. Student's t-test (two-tailed) was used to compare the
503 averages of two groups. Statistical significance was determined at P<0.05 (*), P<0.01 (**), P<0.001
504 (***).
505

506

507 **Acknowledgments**
508
509 We would like to thank G. Kreibich, O. Elroy-Stein, G. Petris and O. Burrone for plasmids and
510 reagents. We are very grateful to F.U. Hartl for ongoing advice and for critically reading and helping
511 in the edition of this manuscript. Work was supported by grant 2577/20 from the Israel Science
512 Foundation (GZL).
513
514 **Author Contributions:** Conceptualization: GZL. Investigation: MS, NO-S, CP, BG, S.S., RK.
515 Bioinformatics: MPC. Supervision: GZL. Writing: GZL. Review and editing: GZL, MS, MPC, RK.

516
517 **Declaration of Interests:** The authors declare no competing interests.

518
519 **References**
520

521 1. Sun, Z., and Brodsky, J.L. (2019). Protein quality control in the secretory pathway. J Cell
522 Biol *218*, 3171-3187. 10.1083/jcb.201906047.
523 2. Wu, X., and Rapoport, T.A. (2018). Mechanistic insights into ER-associated protein
524 degradation. Curr Opin Cell Biol *53*, 22-28. 10.1016/j.ceb.2018.04.004.
525 3. Christianson, J.C., Jarosch, E., and Sommer, T. (2023). Mechanisms of substrate
526 processing during ER-associated protein degradation. Nat Rev Mol Cell Biol *24*, 777-796.
527 10.1038/s41580-023-00633-8.
528 4. Lopata, A., Kniss, A., Löhr, F., Rogov, V.V., and Dötsch, V. (2020). Ubiquitination in the
529 ERAD Process. Int J Mol Sci *21*. 10.3390/ijms21155369.
530 5. Berner, N., Reutter, K.R., and Wolf, D.H. (2018). Protein Quality Control of the
531 Endoplasmic Reticulum and Ubiquitin-Proteasome-Triggered Degradation of Aberrant
532 Proteins: Yeast Pioneers the Path. Annu Rev Biochem *87*, 751-782. 10.1146/annurev-
533 biochem-062917-012749.
534 6. Kikkert, M., Doolman, R., Dai, M., Avner, R., Hassink, G., van Voorden, S., Thanedar, S.,
535 Roitelman, J., Chau, V., and Wiertz, E. (2004). Human HRD1 is an E3 ubiquitin ligase
536 involved in degradation of proteins from the endoplasmic reticulum. J Biol Chem *279*,
537 3525-3534. 10.1074/jbc.M307453200.
538 7. Schoebel, S., Mi, W., Stein, A., Ovchinnikov, S., Pavlovicz, R., DiMaio, F., Baker, D.,
539 Chambers, M.G., Su, H., Li, D., et al. (2017). Cryo-EM structure of the protein-conducting
540 ERAD channel Hrd1 in complex with Hrd3. Nature *548*, 352-355. 10.1038/nature23314.
541 8. Wu, X., Siggel, M., Ovchinnikov, S., Mi, W., Svetlov, V., Nudler, E., Liao, M., Hummer, G.,
542 and Rapoport, T.A. (2020). Structural basis of ER-associated protein degradation
543 mediated by the Hrd1 ubiquitin ligase complex. Science *368*. 10.1126/science.aaz2449.
544 9. Peterson, B.G., Glaser, M.L., Rapoport, T.A., and Baldridge, R.D. (2019). Cycles of
545 autoubiquitination and deubiquitination regulate the ERAD ubiquitin ligase Hrd1. Elife *8*.
546 10.7554/eLife.50903.
547 10. Vasic, V., Denkert, N., Schmidt, C.C., Riedel, D., Stein, A., and Meinecke, M. (2020). Hrd1
548 forms the retrotranslocation pore regulated by auto-ubiquitination and binding of
549 misfolded proteins. Nat Cell Biol *22*, 274-281. 10.1038/s41556-020-0473-4.
550 11. Leitman, J., Shenkman, M., Gofman, Y., Shtern, N.O., Ben-Tal, N., Hendershot, L.M., and
551 Lederkremer, G.Z. (2014). Herp coordinates compartmentalization and recruitment of
552 HRD1 and misfolded proteins for ERAD. Molecular biology of the cell *25*, 1050-1060.
553 10.1091/mbc.E13-06-0350.
554 12. Shenkman, M., and Lederkremer, G.Z. (2019). Compartmentalization and Selective
555 Tagging for Disposal of Misfolded Glycoproteins. Trends Biochem Sci *44*, 827-836.
556 10.1016/j.tibs.2019.04.012.
557 13. Denic, V., Quan, E.M., and Weissman, J.S. (2006). A luminal surveillance complex that
558 selects misfolded glycoproteins for ER-associated degradation. Cell *126*, 349-359.
559 10.1016/j.cell.2006.05.045.
560 14. Mueller, B., Klemm, E.J., Spooner, E., Claessen, J.H., and Ploegh, H.L. (2008). SEL1L
561 nucleates a protein complex required for dislocation of misfolded glycoproteins. Proc
562 Natl Acad Sci U S A *105*, 12325-12330. 10.1073/pnas.0805371105.
563 15. Christianson, J.C., Olzmann, J.A., Shaler, T.A., Sowa, M.E., Bennett, E.J., Richter, C.M.,
564 Tyler, R.E., Greenblatt, E.J., Wade Harper, J., and Kopito, R.R. (2012). Defining human

565 ERAD networks through an integrative mapping strategy. Nature Cell Biology *14*, 93-105.
566 10.1038/ncb2383.
567 16. Hwang, J., Walczak, C.P., Shaler, T.A., Olzmann, J.A., Zhang, L., Elias, J.E., and Kopito, R.R.
568 (2017). Characterization of protein complexes of the endoplasmic reticulum-associated
569 degradation E3 ubiquitin ligase Hrd1. J Biol Chem *292*, 9104-9116.
570 10.1074/jbc.M117.785055.
571 17. Kny, M., Standera, S., Hartmann-Petersen, R., Kloetzel, P.M., and Seeger, M. (2011).
572 Herp regulates Hrd1-mediated ubiquitylation in a ubiquitin-like domain-dependent
573 manner. J Biol Chem *286*, 5151-5156. 10.1074/jbc.M110.134551.
574 18. Cherepanova, N., Shrimal, S., and Gilmore, R. (2016). N-linked glycosylation and
575 homeostasis of the endoplasmic reticulum. Curr Opin Cell Biol *41*, 57-65.
576 10.1016/j.ceb.2016.03.021.
577 19. Mohanty, S., Chaudhary, B.P., and Zoetewey, D. (2020). Structural Insight into the
578 Mechanism of N-Linked Glycosylation by Oligosaccharyltransferase. Biomolecules *10*.
579 10.3390/biom10040624.
580 20. Qin, S.Y., Hu, D., Matsumoto, K., Takeda, K., Matsumoto, N., Yamaguchi, Y., and
581 Yamamoto, K. (2012). Malectin forms a complex with ribophorin I for enhanced
582 association with misfolded glycoproteins. J Biol Chem *287*, 38080-38089.
583 10.1074/jbc.M112.394288.
584 21. Wilson, C.M., Kraft, C., Duggan, C., Ismail, N., Crawshaw, S.G., and High, S. (2005).
585 Ribophorin I associates with a subset of membrane proteins after their integration at
586 the sec61 translocon. J Biol Chem *280*, 4195-4206. 10.1074/jbc.M410329200.
587 22. Shenkman, M., Ayalon, M., and Lederkremer, G.Z. (1997). Endoplasmic reticulum quality
588 control of asialoglycoprotein receptor H2a involves a determinant for retention and not
589 retrieval. Proc Natl Acad Sci U S A *94*, 11363-11368. 10.1073/pnas.94.21.11363.
590 23. Groisman, B., Shenkman, M., Ron, E., and Lederkremer, G.Z. (2011). Mannose trimming
591 is required for delivery of a glycoprotein from EDEM1 to XTP3-B and to late endoplasmic
592 reticulum-associated degradation steps. J Biol Chem *286*, 1292-1300.
593 10.1074/jbc.M110.154849.
594 24. Kondratyev, M., Avezov, E., Shenkman, M., Groisman, B., and Lederkremer, G.Z. (2007).
595 PERK-dependent compartmentalization of ERAD and unfolded protein response
596 machineries during ER stress. Exp Cell Res *313*, 3395-3407. 10.1016/j.yexcr.2007.07.006.
597 25. Keefe, A.D., Wilson, D.S., Seelig, B., and Szostak, J.W. (2001). One-step purification of
598 recombinant proteins using a nanomolar-affinity streptavidin-binding peptide, the SBP-
599 Tag. Protein Expr Purif *23*, 440-446.
600 26. Adelman, M.R., Sabatini, D.D., and Blobel, G. (1973). Ribosome-membrane interaction.
601 Nondestructive disassembly of rat liver rough microsomes into ribosomal and
602 membranous components. J Cell Biol *56*, 206-229. 10.1083/jcb.56.1.206.
603 27. Ogen-Shtern, N., Chang, C., Saad, H., Mazkereth, N., Patel, C., Shenkman, M., and
604 Lederkremer, G.Z. (2023). COP I and II dependent trafficking controls ER-associated
605 degradation in mammalian cells. iScience *26*, 106232. 10.1016/j.isci.2023.106232.
606 28. Pfeffer, S., Dudek, J., Gogala, M., Schorr, S., Linxweiler, J., Lang, S., Becker, T., Beckmann,
607 R., Zimmermann, R., and Förster, F. (2014). Structure of the mammalian oligosaccharyl-
608 transferase complex in the native ER protein translocon. Nat Commun *5*, 3072.
609 10.1038/ncomms4072.
610 29. Scotter, E.L., Vance, C., Nishimura, A.L., Lee, Y.B., Chen, H.J., Urwin, H., Sardone, V.,
611 Mitchell, J.C., Rogelj, B., Rubinsztein, D.C., and Shaw, C.E. (2014). Differential roles of the

612 ubiquitin proteasome system and autophagy in the clearance of soluble and aggregated
613 TDP-43 species. J Cell Sci *127*, 1263-1278. 10.1242/jcs.140087.
614 30. Kelleher, D.J., and Gilmore, R. (1997). DAD1, the defender against apoptotic cell death,
615 is a subunit of the mammalian oligosaccharyltransferase. Proc Natl Acad Sci U S A *94*,
616 4994-4999.
617 31. Nikonov, A.V., Snapp, E., Lippincott-Schwartz, J., and Kreibich, G. (2002). Active
618 translocon complexes labeled with GFP-Dad1 diffuse slowly as large polysome arrays in
619 the endoplasmic reticulum. J Cell Biol *158*, 497-506. 10.1083/jcb.200201116.
620 32. Kamhi-Nesher, S., Shenkman, M., Tolchinsky, S., Fromm, S.V., Ehrlich, R., and
621 Lederkremer, G.Z. (2001). A novel quality control compartment derived from the
622 endoplasmic reticulum. Molecular biology of the cell *12*, 1711-1723.
623 10.1091/mbc.12.6.1711.
624 33. Frenkel, Z., Shenkman, M., Kondratyev, M., and Lederkremer, G.Z. (2004). Separate roles
625 and different routing of calnexin and ERp57 in endoplasmic reticulum quality control
626 revealed by interactions with asialoglycoprotein receptor chains. Mol Biol Cell *15*, 2133-
627 2142. 10.1091/mbc.e03-12-0899.
628 34. Pereira, F., Rettel, M., Stein, F., Savitski, M.M., Collinson, I., and Römisch, K. (2019).
629 Effect of Sec61 interaction with Mpd1 on endoplasmic reticulum-associated
630 degradation. PLoS One *14*, e0211180. 10.1371/journal.pone.0211180.
631 35. Ron, E., Shenkman, M., Groisman, B., Izenshtein, Y., Leitman, J., and Lederkremer, G.Z.
632 (2011). Bypass of glycan-dependent glycoprotein delivery to ERAD by up-regulated
633 EDEM1. Molecular biology of the cell *22*, 3945-3954. mbc.E10-12-0944 [pii]

634 10.1091/mbc.E10-12-0944 [doi].
635 36. Benyair, R., Ogen-Shtern, N., Mazkereth, N., Shai, B., Ehrlich, M., and Lederkremer, G.Z.
636 (2015). Mammalian ER mannosidase I resides in quality control vesicles, where it
637 encounters its glycoprotein substrates. Molecular biology of the cell *26*, 172-184.
638 10.1091/mbc.E14-06-1152.
639 37. Shenkman, M., Groisman, B., Ron, E., Avezov, E., Hendershot, L.M., and Lederkremer,
640 G.Z. (2013). A Shared Endoplasmic Reticulum-associated Degradation Pathway Involving
641 the EDEM1 Protein for Glycosylated and Nonglycosylated Proteins. J Biol Chem *288*,
642 2167-2178. M112.438275 [pii]

643 10.1074/jbc.M112.438275 [doi].
644 38. Lamriben, L., Oster, M.E., Tamura, T., Tian, W., Yang, Z., Clausen, H., and Hebert, D.N.
645 (2018). EDEM1's mannosidase-like domain binds ERAD client proteins in a redox-
646 sensitive manner and possesses catalytic activity. J Biol Chem *293*, 13932-13945.
647 10.1074/jbc.RA118.004183.
648 39. Petris, G., Vecchi, L., Bestagno, M., and Burrone, O.R. (2011). Efficient detection of
649 proteins retro-translocated from the ER to the cytosol by in vivo biotinylation. PLoS One
650 *6*, e23712. 10.1371/journal.pone.0023712.
651 40. Sharma, N., Patel, C., Shenkman, M., Kessel, A., Ben-Tal, N., and Lederkremer, G.Z.
652 (2021). The Sigma-1 receptor is an ER-localized type II membrane protein. J Biol Chem
653 *297*, 101299. 10.1016/j.jbc.2021.101299.
654 41. Ramírez, A.S., Kowal, J., and Locher, K.P. (2019). Cryo-electron microscopy structures of
655 human oligosaccharyltransferase complexes OST-A and OST-B. Science *366*, 1372-1375.
656 10.1126/science.aaz3505.

657 42. Newport, T.D., Sansom, M.S.P., and Stansfeld, P.J. (2019). The MemProtMD database: a
658 resource for membrane-embedded protein structures and their lipid interactions.
659 Nucleic Acids Res *47*, D390-d397. 10.1093/nar/gky1047.
660 43. Wu, X., and Rapoport, T.A. (2021). Translocation of Proteins through a Distorted Lipid
661 Bilayer. Trends Cell Biol *31*, 473-484. 10.1016/j.tcb.2021.01.002.
662 44. Shibatani, T., David, L.L., McCormack, A.L., Frueh, K., and Skach, W.R. (2005). Proteomic
663 analysis of mammalian oligosaccharyltransferase reveals multiple subcomplexes that
664 contain Sec61, TRAP, and two potential new subunits. Biochemistry *44*, 5982-5992.
665 10.1021/bi047328f.
666 45. Losfeld, M.E., Ng, B.G., Kircher, M., Buckingham, K.J., Turner, E.H., Eroshkin, A., Smith,
667 J.D., Shendure, J., Nickerson, D.A., Bamshad, M.J., et al. (2014). A new congenital
668 disorder of glycosylation caused by a mutation in SSR4, the signal sequence receptor 4
669 protein of the TRAP complex. Human Molecular Genetics *23*, 1602-1605.
670 10.1093/hmg/ddt550.
671 46. Nagasawa, K., Higashi, T., Hosokawa, N., Kaufman, R.J., and Nagata, K. (2007).
672 Simultaneous induction of the four subunits of the TRAP complex by ER stress
673 accelerates ER degradation. EMBO Rep *8*, 483-489. 10.1038/sj.embor.7400933.
674 47. Russo, A. (2020). Understanding the mammalian TRAP complex function(s). Open Biol
675 *10*, 190244. 10.1098/rsob.190244.
676 48. Yamamoto, S., Yamazaki, T., Komazaki, S., Yamashita, T., Osaki, M., Matsubayashi, M.,
677 Kidoya, H., Takakura, N., Yamazaki, D., and Kakizawa, S. (2014). Contribution of calumin
678 to embryogenesis through participation in the endoplasmic reticulum-associated
679 degradation activity. Dev Biol *393*, 33-43. 10.1016/j.ydbio.2014.06.024.
680 49. Kon, T., Mori, F., Tanji, K., Miki, Y., Nishijima, H., Nakamura, T., Kinoshita, I., Suzuki, C.,
681 Kurotaki, H., Tomiyama, M., and Wakabayashi, K. (2022). Accumulation of Nonfibrillar
682 TDP-43 in the Rough Endoplasmic Reticulum Is the Early-Stage Pathology in
683 Amyotrophic Lateral Sclerosis. J Neuropathol Exp Neurol *81*, 271-281.
684 10.1093/jnen/nlac015.
685 50. Lin, D.L., Cherepanova, N.A., Bozzacco, L., MacDonald, M.R., Gilmore, R., and Tai, A.W.
686 (2017). Dengue Virus Hijacks a Noncanonical Oxidoreductase Function of a Cellular
687 Oligosaccharyltransferase Complex. mBio *8*. 10.1128/mBio.00939-17.
688 51. Patel, C., Saad, H., Shenkman, M., and Lederkremer, G.Z. (2020). Oxidoreductases in
689 Glycoprotein Glycosylation, Folding, and ERAD. Cells *9*. 10.3390/cells9092138.
690 52. Cherepanova, N.A., Shrimal, S., and Gilmore, R. (2014). Oxidoreductase activity is
691 necessary for N-glycosylation of cysteine-proximal acceptor sites in glycoproteins. J Cell
692 Biol *206*, 525-539. 10.1083/jcb.201404083.
693 53. Lilley, B.N., and Ploegh, H.L. (2004). A membrane protein required for dislocation of
694 misfolded proteins from the ER. Nature *429*, 834-840. 10.1038/nature02592.
695 54. Christianson, J.C., Shaler, T.A., Tyler, R.E., and Kopito, R.R. (2008). OS-9 and GRP94
696 deliver mutant alpha1-antitrypsin to the Hrd1-SEL1L ubiquitin ligase complex for ERAD.
697 Nat Cell Biol *10*, 272-282. 10.1038/ncb1689.
698 55. Cherepanova, N.A., and Gilmore, R. (2016). Mammalian cells lacking either the
699 cotranslational or posttranslocational oligosaccharyltransferase complex display
700 substrate-dependent defects in asparagine linked glycosylation. Sci Rep *6*, 20946.
701 10.1038/srep20946.
702 56. Knopf, J.D., Landscheidt, N., Pegg, C.L., Schulz, B.L., Kühnle, N., Chao, C.W., Huck, S., and
703 Lemberg, M.K. (2020). Intramembrane protease RHBDL4 cleaves

704 oligosaccharyltransferase subunits to target them for ER-associated degradation. J Cell
705 Sci *133*. 10.1242/jcs.243790.
706 57. Hosokawa, N., Wada, I., Nagasawa, K., Moriyama, T., Okawa, K., and Nagata, K. (2008).
707 Human XTP3-B forms an endoplasmic reticulum quality control scaffold with the HRD1-
708 SEL1L ubiquitin ligase complex and BiP. J Biol Chem *283*, 20914-20924.
709 10.1074/jbc.M709336200.
710 58. Jaenicke, L.A., Brendebach, H., Selbach, M., and Hirsch, C. (2011). Yos9p assists in the
711 degradation of certain nonglycosylated proteins from the endoplasmic reticulum.
712 Molecular biology of the cell *22*, 2937-2945. 10.1091/mbc.E10-10-0832.
713 59. Tolchinsky, S., Yuk, M.H., Ayalon, M., Lodish, H.F., and Lederkremer, G.Z. (1996).
714 Membrane-bound versus secreted forms of human asialoglycoprotein receptor subunits
715 - Role of a juxtamembrane pentapeptide. J Biol Chem *271*, 14496-14503.
716 10.1074/jbc.271.24.14496.
717 60. Ogen-Shtern, N., Avezov, E., Shenkman, M., Benyair, R., and Lederkremer, G.Z. (2016).
718 Mannosidase IA is in Quality Control Vesicles and Participates in Glycoprotein Targeting
719 to ERAD. Journal of molecular biology *428*, 3194-3205. 10.1016/j.jmb.2016.04.020.
720 61. Avezov, E., Frenkel, Z., Ehrlich, M., Herscovics, A., and Lederkremer, G.Z. (2008).
721 Endoplasmic reticulum (ER) mannosidase I is compartmentalized and required for N-
722 glycan trimming to Man5-6GlcNAc2 in glycoprotein ER-associated degradation. Mol Biol
723 Cell *19*, 216-225. 10.1091/mbc.e07-05-0505.
724 62. Leitman, J., Ulrich Hartl, F., and Lederkremer, G.Z. (2013). Soluble forms of polyQ-
725 expanded huntingtin rather than large aggregates cause endoplasmic reticulum stress.
726 Nature Communications *4*, 2753. 10.1038/ncomms3753.
727 63. Call, M.E., Pyrdol, J., Wiedmann, M., and Wucherpfennig, K.W. (2002). The organizing
728 principle in the formation of the T cell receptor-CD3 complex. Cell *111*, 967-979.
729 64. Sherman, B.T., Hao, M., Qiu, J., Jiao, X., Baseler, M.W., Lane, H.C., Imamichi, T., and
730 Chang, W. (2022). DAVID: a web server for functional enrichment analysis and functional
731 annotation of gene lists (2021 update). Nucleic Acids Res *50*, W216-w221.
732 10.1093/nar/gkac194.
733 65. Szklarczyk, D., Kirsch, R., Koutrouli, M., Nastou, K., Mehryary, F., Hachilif, R., Gable, A.L.,
734 Fang, T., Doncheva, N.T., Pyysalo, S., et al. (2023). The STRING database in 2023:
735 protein-protein association networks and functional enrichment analyses for any
736 sequenced genome of interest. Nucleic Acids Res *51*, D638-d646.
737 10.1093/nar/gkac1000.

738

739

740 **Figure legends**

741 **Fig. 1. OST subunits are among top ERAD substrate interactors identified by a SILAC**
742 **proteomics approach. (a)** Experimental scheme of SILAC-based mass spectrometry analysis of
743 HEK293 cells labeled with lysine containing heavy isotopes for 10 days or HEK293 stably
744 expressing H2aSBP (SBP6 cell line) without heavy lysine (or vice versa). Cells were treated with
745 MG-132 (50μM) and ALLN (50μM) for 4h and puromycin (2mM) for 15 min before lysis, or only
746 with puromycin. Cells were solubilized in 1% digitonin in PBS and lysates from cells labeled with
747 or without heavy lysine were mixed 1:1. Protein complexes pulled down with H2aSBP (using
748 streptavidin-agarose beads) were eluted with 250μM biotin, subjected to SDS-PAGE followed by
749 trypsin digestion and LC-MS/MS analysis. **(b)** Effect of mutant HRD1 on H2aSBP. Dominant
750 negative mutant myc-tagged hsHRD1 (mutHRD1-myc) was transfected into SBP6 cells. Two
751 days post-transfection these cells or control HEK293 cells were treated or not for 4h with 20 μM
752 MG132, lysed and subjected to precipitation with streptavidin beads. Biotin-eluted samples were
753 subjected to 10% SDS-PAGE and immunoblotted with anti-H2a or anti-myc. MW markers in kDa
754 are on the right. **(c)** Metabolically labeled proteins pulled down with H2aSBP. SBP6 cells or
755 control HEK293 cells were labeled with [^{35}S] Cys/Met mix for 5h under proteasomal inhibition with
756 20mM MG132 and treated or not with 2mM puromycin for the last 15 min before lysis. Cells were
757 lysed in digitonin buffer followed by precipitation with streptavidin beads, elution with biotin and
758 SDS-PAGE with detection by fluorography. **(d)** Proteins pulled down with H2aSBP and silver
759 stained. SBP6 cells or control HEK293 cells were treated for 4h with 20μM MG132 and 2mM
760 puromycin (last 15 min), lysed in digitonin buffer followed by precipitation with streptavidin beads
761 (in the presence of 0.1% BSA), elution with biotin, SDS-PAGE and silver staining. **(e)** Gene
762 Ontology (GO) analysis of differentially expressed genes from the SILAC results of cells with or
763 without proteasomal inhibition (ratio>1.5). -log2 enriched p-values are shown for selected top
764 entries with the lowest false discovery rates. (see also Suppl. Table 1). **(f)** STRING interaction
765 map of proteins identified in the SILAC analysis, highlighting those with >1.5 ratio when
766 comparing cells treated with or without proteasomal inhibitors. OST protein subunits are in red,
767 other enriched functions are in colored circles. **(g)** Ratio of levels of proteins identified in cells
768 treated with or without proteasomal inhibitors. The proteins on the left (up to UBQL2) were
769 detected only in proteasomal inhibitor-treated cells. The dotted line is a value of 1, equal
770 presence in cells treated with or without proteasomal inhibitors. (see also Suppl. Tables 2 and 3).

771

772 **Fig. 2. DAD1 accumulates in the ERQC upon proteasomal inhibition separately from**
773 **ribosomes and interacts increasingly with an ERAD substrate. (a-d)** GFP-DAD1 and
774 Sec61β-GFP accumulate at the ERQC. NIH 3T3 cells were transiently cotransfected with the
775 ERAD substrate H2a-RFP and with GFP-DAD1 or Sec61β-GFP and were incubated with or
776 without 17 μM Lac for 3h. **(e-f)** Ribosomes do not accumulate at the ERQC. NIH 3T3 cells
777 transiently transfected with H2a-RFP were treated as in (a-d) and were fixed and immunostained
778 using a primary mouse anti-rRNA antibody and secondary goat anti-mouse IgG antibody
779 conjugated to Cy2. **(g-l)** GFP-DAD1 colocalizes with OS-9 with or without proteasomal inhibition.
780 S-tagged OS-9.1/2 was expressed in NIH 3T3 cells together with H2a-GFP or GFP-DAD1, with or
781 without treatment with 1.5 μM Bz for 3h, followed by fixation and immunostaining with mouse anti-
782 S tag antibody and secondary goat anti-mouse IgG antibody conjugated to Dylight 549. The
783 graphs are from data from 3 repeat experiments. **(m)** Comigration of endogenous DAD1 and the
784 ERAD substrate at the ERQC. HEK293 cells transiently transfected with H2a-RFP were
785 incubated without (left) or with Bz (2 μM) for 3 h. Cells were homogenized and postnuclear
786 supernatants were centrifuged on 10–34% iodixanol gradients. Fractions of the gradients were
787 run on SDS–PAGE and immunoblotted with the indicated antibodies. H2a-RFP was detected with
788 anti-RFP. A representative experiment out of 3 repeat experiments is shown. **(n)**
789 Immunoprecipitation with a mouse monoclonal (B9) anti-H2a of lysates of HEK293 cells
790 expressing H2a together with GFP-DAD1, with or without treatment with 2 μM Bz for 3 h.
791 Crosslinking with 1 mM DSP was performed before cell lysis. Immunoprecipitates and 10% of the

792 total lysates (input) were immunoblotted with rabbit anti-H2a amino-terminal antibody and anti-
793 GFP. Asterisk= non-specific band. The graph shows increased coimmunoprecipitation of GFP-
794 DAD1 with H2a upon proteasomal inhibition. Values are relative to control (=100), normalized by
795 total GFP-DAD1 and H2a, average of 4 independent experiments ±SD. p value = 0.0003.

796

797 **Fig. 3. OST subunits promote degradation of a glycosylated ERAD substrate. (a-c)**
798 Overexpression of GFP-DAD1 strongly reduces the levels of H2a, knockdown of DAD1 or Tusc3
799 increases H2a levels. Cell lysates were immunoblotted with anti-H2a amino-terminal antibody.
800 The graphs show averages of 3 or 4 independent experiments ±SD. p value ±GFP-DAD1 = $2x10^{-}$
801 ^{5}, ±shDAD1 = 0.03, ±shTusc3 = 0.0004. **(d-f)** Pulse-labeling for 20 min with [^{35}S]cysteine and
802 chase for the indicated times of cells expressing H2a with or without overexpression of GFP-
803 DAD1 (d), knockdown of Tusc3 (e) or treatment with Tun (5 μg/ml) for 18h prior to the pulse and
804 during the pulse and chase times (f). H2a degradation (percentage remaining relative to pulse)
805 was accelerated by GFP-DAD1, inhibited by Tusc3 knockdown and was not affected by blocking
806 glycosylation (+Tun). The graphs show averages of 3 independent experiments ±SD. p value
807 ±GFP-DAD1 3h = 0.05, 6h = 0.05; ±shTusc3 3h = 0.03; ±Tun 3h = 0.04.

808

809 **Fig. 4. Participation of OST subunits to a lesser extent in the degradation of an**
810 **unglycosylated ERAD substrate. (a-c)** Overexpression of GFP-DAD1 reduces the levels of
811 H2aDgly, knockdown of DAD1 does not affect its levels whereas Tusc3 knockdown increases
812 moderately H2aDgly levels. Cell lysates were immunoblotted with anti-H2a amino-terminal
813 antibody. The graphs show averages of 3 or 4 independent experiments ±SD. p value ±GFP-
814 DAD1 = $3x10^{-6}$, ±shTusc3 = 0.004. **(d)** Pulse/ chase with [^{35}S]cysteine of cells expressing
815 H2aDgly shows a moderate inhibition of its degradation by Tusc3 knockdown. The graph shows
816 an average of 3 independent experiments ±SD. p value ±shTusc3 3h = 0.01.

817

818 **Fig. 5. OST subunits affect levels of other ERAD substrates. (a-c)** Overexpression of GFP-
819 DAD1 reduces moderately the levels of BACE476-HA, knockdown of DAD1 or Tusc3 cause a
820 minor increase in BACE476-HA levels. Cell lysates were immunoblotted with anti-HA and anti-
821 actin as loading control. **(d-f)** Overexpression of GFP-DAD1 causes a minor reduction in the
822 levels of NHK-HA, knockdown of DAD1 or Tusc3 increase moderately NHK-HA levels. Cell
823 lysates were immunoblotted with anti-HA and anti-β tubulin as loading control. The graphs show
824 averages of 3 independent experiments ±SD. p value for BACE476-HA: ±GFP-DAD1 = 0.008,
825 ±shDAD1 = 0.01, ±shTusc3 = 0.003; for NHK-HA: ±GFP-DAD1 = 0.05, ±shDAD1 = $2x10^{-6}$,
826 ±shTusc3 = 0.03.

827

828 **Fig. 6. Interaction of an OST subunit with HRD1 and promotion of retrotranslocation of an**
829 **ERAD substrate. (a)** Immunoprecipitation with anti-myc of lysates of HEK293 cells expressing
830 HRD1-myc together with GFP-DAD1 and treated with or without 2 μM Bz for 4 h.
831 Immunoprecipitates and 10% of the total lysates (input) were immunoblotted with anti-myc and
832 anti-GFP. The graph shows reduced coimmunoprecipitation of GFP-DAD1 with HRD1-myc under
833 proteasomal inhibition. Values are relative to control (=100), normalized by total GFP-DAD1 and
834 HRD1-myc, average of 3 independent experiments ±SD. p value = 0.009. **(b)** Scheme of addition
835 of biotin (star) to H2a-BAP by an ER luminal biotin ligase, sec-BirA or after retrotranslocation by a
836 cytosolic one, BirA. HEK293 cells transiently expressing H2a-BAP with or without BirA or Sec-
837 BirA were incubated 24h post-transfection with biotin (100μM) for 30 min before lysis. Strep-HRP
838 was used to detect biotinylated H2a-BAP and anti-V5 to detect total H2a-BAP. **(c)** Cells
839 expressing H2a-BAP together with BirA and GFP-DAD1 overexpression or knockdown of DAD1

840 or Tusc3 were incubated with biotin for 3h. Cell lysates were reacted with Strep-HRP or with anti-
841 H2a antibody. Retrotranslocated (biotinylated) H2a-BAP increased almost two-fold under GFP-
842 DAD1 overexpression and was reduced to half under Tusc3 or DAD1 knockdown. Values are
843 averages of 4 independent experiments ±SD, relative to total H2a-BAP and standardized by the
844 control (=100). P value +shTusc3 vs. control = 0.02, +GFP-DAD1 vs. control = 0.04, +shDAD1 vs.
845 control = 0.02.

846 **Fig. 7. Membrane thinning by OST complexes. (a, b)** 3D structures of human
847 oligosaccharyltransferase complexes OST-A and OST-B determined by cryo-EM at 3.5 Å
848 resolution, indicating with different colors the observed subunits and illustrating the topology in
849 the ER in relation to the transmembrane domain (TMD). From the RCSB database (6S7O and
850 6S7T). **(c, d)** Side views of OST-A and OST-B with membrane boundaries from simulations by
851 molecular dynamics pre-rendered at the MemProtMD database. Distortions of the lipid bilayer
852 indicate considerable membrane thinning by the OST transmembrane domains, highlighted by
853 red lipid phosphate head groups, whereas blue illustrates thickening. **(e)** Model illustrating the
854 interaction of OST with translocon components during forward translocation and its participation
855 in N-glycosylation. OST also interacts with HRD1 and participates in retrotranslocation and
856 targeting to ERAD.

857

858 **Table 1**

859

OST subunit	**UNIPROT Accession No.**	**Hit No.**	**Median ratio with vs. without proteasome inhibition**	**Peptides (seq)**	**Sequence Coverage (%)**
IAP/ MAGT1, MAGT1_HUMAN	Q9H0U3		Only in cells treated with proteasome inhibitors	4	10.1
STT3 A, STT3A_HUMAN	P46977		Only in cells treated with proteasome inhibitors	8	11.2
DC2/ OSTC, OSATC_HUMAN	Q9NRP0		Only in cells treated with proteasome inhibitors	1	8.1
Ribophorin II, RPN2_HUMAN	P04844	27	4.3	15	30.9
OST 48, OST48_HUMAN	P39656	32	2.8	11	29.8
Ribophorin I, RPN1_HUMAN	P04843	36	2.4	18	32.5

860

861 **Table 1. OST subunits detected by mass spectrometry.** LC-MS/MS analysis following the
862 experimental scheme of Fig. 1a. Results of >2 fold labeled/unlabeled from cells treated with MG-

863 132 and ALLN for 4h and puromycin for 15 min before lysis were compared to those from cells
864 treated with only puromycin for 15 min, after normalization to the total amount of H2a-SBP
865 (ASGPR2, bait) obtained. Hits are ranked by enrichment in cells treated with vs. without
866 proteasome inhibitors. Only OST subunits, with enrichment values of 2-fold or higher in cells
867 treated with vs. without proteasome inhibitors or found only in cells treated with proteasome
868 inhibitors are shown. See Suppl. Tables 2 and 3 for complete lists of hits.

869

Fig. 1

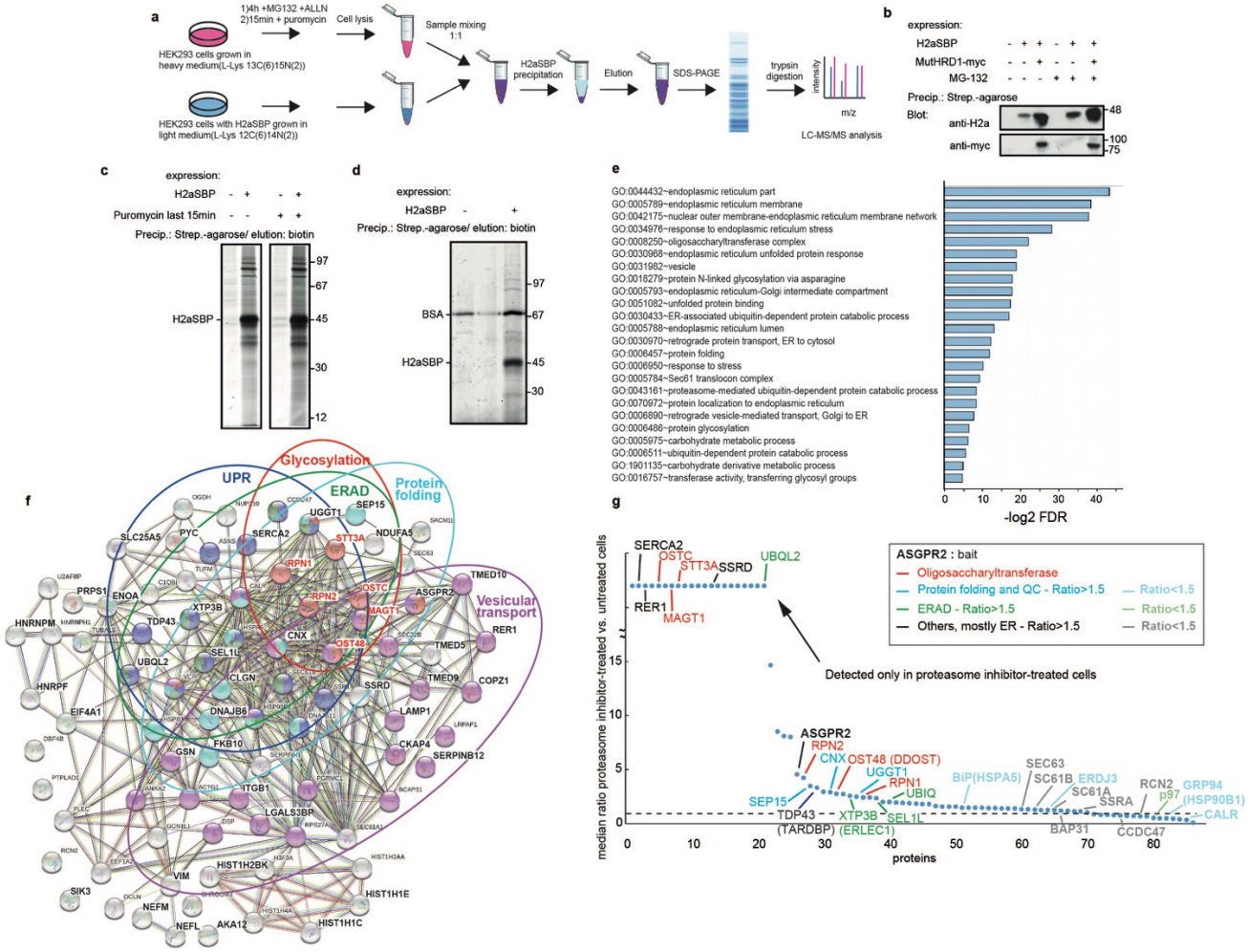
a
1)4h +MG132 +ALLN
2)15min + puromycin
Cell lysis
Sample mixing
1:1
H2aSBP
precipitation
Elution
SDS-PAGE
trypsin
digestion
intensity
m/z
LC-MS/MS analysis
HEK293 cells grown in
heavy medium(L-Lys 13C(6)15N(2))
HEK293 cells with H2aSBP grown in
light medium(L-Lys 12C(6)14N(2))
b
expression:
H2aSBP
MutHRD1-myc
MG-132
Precip.: Strep.-agarose
Blot:
anti-H2a
anti-myc
48
100
75
c
expression:
H2aSBP
Puromycin last 15min
Precip.: Strep.-agarose/ elution: biotin
H2aSBP
97
67
45
30
12
d
expression:
H2aSBP
Precip.: Strep.-agarose/ elution: biotin
BSA
H2aSBP
97
67
45
30
e
GO:0044432~endoplasmic reticulum part
GO:0005789~endoplasmic reticulum membrane
GO:0042175~nuclear outer membrane-endoplasmic reticulum membrane network
GO:0034976~response to endoplasmic reticulum stress
GO:0008250~oligosaccharyltransferase complex
GO:0030968~endoplasmic reticulum unfolded protein response
GO:0031982~vesicle
GO:0018279~protein N-linked glycosylation via asparagine
GO:0005793~endoplasmic reticulum-Golgi intermediate compartment
GO:0051082~unfolded protein binding
GO:0030433~ER-associated ubiquitin-dependent protein catabolic process
GO:0005788~endoplasmic reticulum lumen
GO:0030970~retrograde protein transport, ER to cytosol
GO:0006457~protein folding
GO:0006950~response to stress
GO:0005784~Sec61 translocon complex
GO:0043161~proteasome-mediated ubiquitin-dependent protein catabolic process
GO:0070972~protein localization to endoplasmic reticulum
GO:0006890~retrograde vesicle-mediated transport, Golgi to ER
GO:0006486~protein glycosylation
GO:0005975~carbohydrate metabolic process
GO:0006511~ubiquitin-dependent protein catabolic process
GO:1901135~carbohydrate derivative metabolic process
GO:0016757~transferase activity, transferring glycosyl groups
0
10
20
30
40
-log2 FDR
f
UPR
Glycosylation
ERAD
Protein folding
Vesicular transport
SLC25A5
PYC
SERCA2
UGGT1
SEP15
STT3A
NDUFA5
RPN1
RPN2
OSTC
MAGT1
ASGPR2
TMED10
ENOA
PRPS1
XTP3B
TDP43
HNRNPM
CNX
OST48
SEL1L
UBQL2
CLGN
TMED5
TMED9
RER1
COPZ1
SSRD
HNRPF
EIF4A1
DNAJB6
LAMP1
FKB10
CKAP4
GSN
SERPINB12
ITGB1
LGALS3BP
VIM
HIST1H2BK
HIST1H1E
SIK3
NEFM
NEFL
AKA12
HIST1H1C
g
SERCA2
OSTC
STT3A
SSRD
UBQL2
RER1
MAGT1
ASGPR2 : bait
Oligosaccharyltransferase
Protein folding and QC - Ratio>1.5
ERAD - Ratio>1.5
Others, mostly ER - Ratio>1.5
Ratio<1.5
Ratio<1.5
Ratio<1.5
Detected only in proteasome inhibitor-treated cells
ASGPR2
RPN2
CNX
OST48 (DDOST)
UGGT1
RPN1
UBIQ
SEP15
TDP43
(TARDBP)
XTP3B
(ERLEC1)
SEL1L
BiP(HSPA5)
SEC63
SC61B
ERDJ3
SC61A
SSRA
RCN2
p57
GRP94
(HSP90B1)
CALR
BAP31
CCDC47
median ratio proteasome inhibitor-treated vs. untreated cells
proteins
0
5
15
0
10
20
30
40
50
60
70
80

870

871

Fig. 2

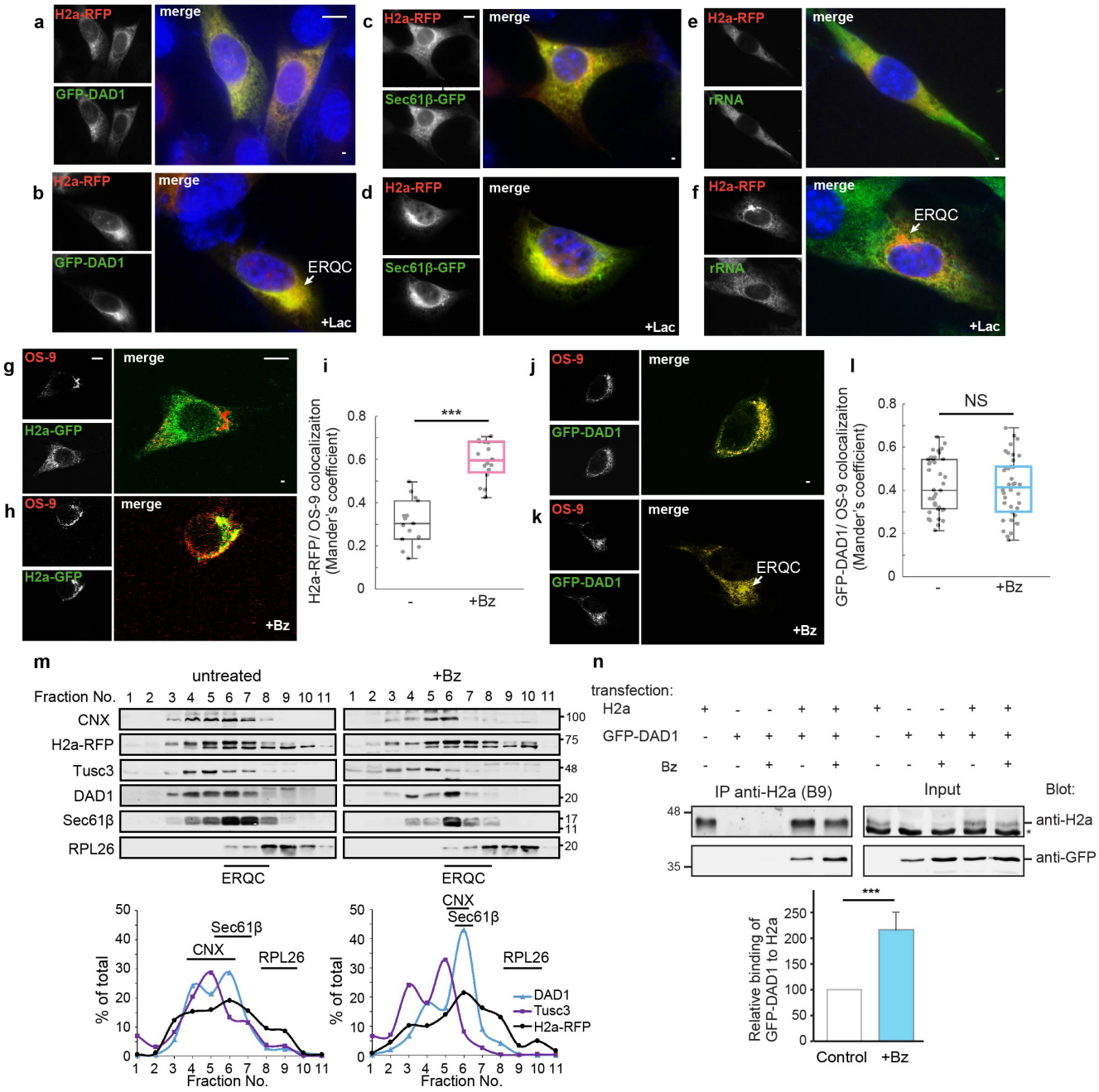
a
H2a-RFP
GFP-DAD1
merge
b
H2a-RFP
GFP-DAD1
merge
ERQC
+Lac
c
H2a-RFP
Sec61β-GFP
merge
d
H2a-RFP
Sec61β-GFP
merge
+Lac
e
H2a-RFP
rRNA
merge
f
H2a-RFP
rRNA
merge
ERQC
+Lac
g
OS-9
H2a-GFP
merge
h
OS-9
H2a-GFP
merge
+Bz
i
H2a-RFP/ OS-9 colocalizaiton (Mander's coefficient)
***
-
+Bz
j
OS-9
GFP-DAD1
merge
k
OS-9
GFP-DAD1
merge
ERQC
+Bz
l
GFP-DAD1/ OS-9 colocalizaiton (Mander's coefficient)
NS
-
+Bz
m
untreated
+Bz
Fraction No.
CNX
H2a-RFP
Tusc3
DAD1
Sec61β
RPL26
ERQC
% of total
Fraction No.
DAD1
Tusc3
H2a-RFP
n
transfection:
H2a
GFP-DAD1
Bz
IP anti-H2a (B9)
Input
Blot:
anti-H2a
anti-GFP
Relative binding of GFP-DAD1 to H2a
Control
+Bz

Fig. 3

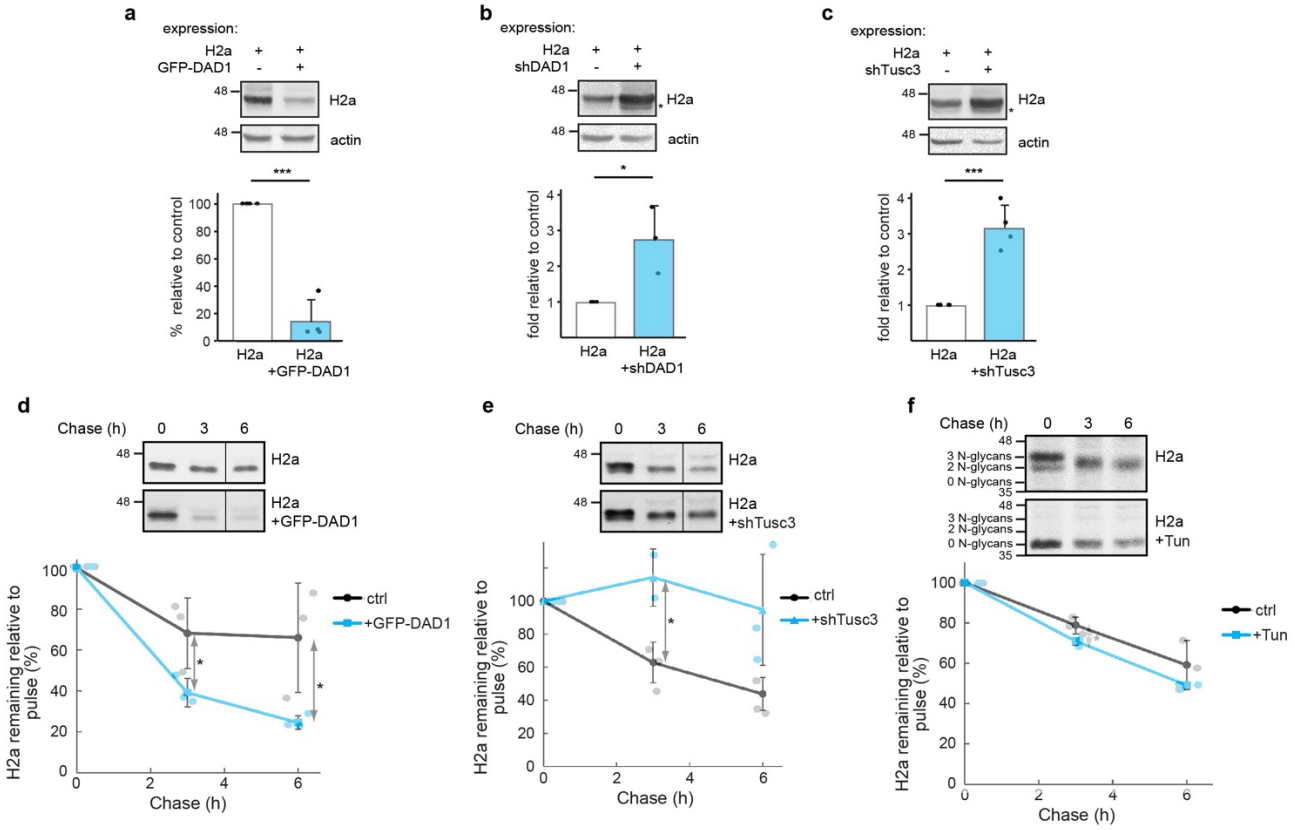
a
expression:
H2a + +
GFP-DAD1 - +
48
H2a
48
actin
***
% relative to control
100
80
60
40
20
0
H2a
H2a +GFP-DAD1
b
expression:
H2a + +
shDAD1 - +
48
H2a
48
actin
*
fold relative to control
4
3
2
1
H2a
H2a +shDAD1
c
expression:
H2a + +
shTusc3 - +
48
H2a
48
actin
***
fold relative to control
4
3
2
1
H2a
H2a +shTusc3
d
Chase (h) 0 3 6
48
H2a
48
H2a +GFP-DAD1
H2a remaining relative to pulse (%)
100
80
60
40
20
0
0 2 4 6
Chase (h)
ctrl
+GFP-DAD1
*
*
e
Chase (h) 0 3 6
48
H2a
48
H2a +shTusc3
H2a remaining relative to pulse (%)
100
80
60
40
20
0
0 2 4 6
Chase (h)
ctrl
+shTusc3
*
f
Chase (h) 0 3 6
48
3 N-glycans
2 N-glycans
0 N-glycans
35
H2a
48
3 N-glycans
2 N-glycans
0 N-glycans
35
H2a +Tun
H2a remaining relative to pulse (%)
100
80
60
40
20
0
0 2 4 6
Chase (h)
ctrl
+Tun

874

Fig. 4

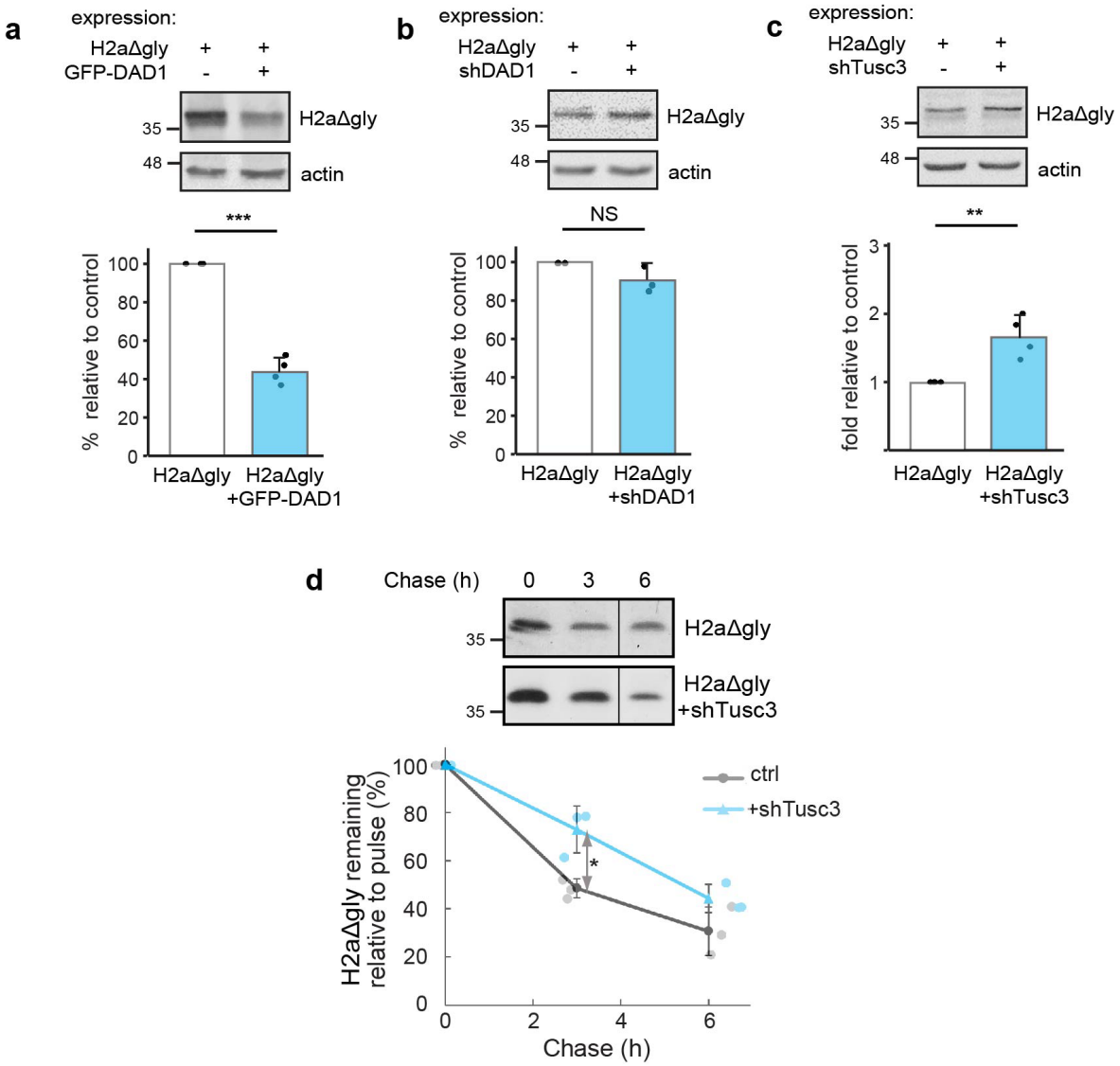
a
expression:
H2aΔgly + +
GFP-DAD1 - +
35
48
H2aΔgly
actin
***
% relative to control
100
80
60
40
20
0
H2aΔgly
H2aΔgly +GFP-DAD1
b
expression:
H2aΔgly + +
shDAD1 - +
35
48
H2aΔgly
actin
NS
% relative to control
100
80
60
40
20
0
H2aΔgly
H2aΔgly +shDAD1
c
expression:
H2aΔgly + +
shTusc3 - +
35
48
H2aΔgly
actin
**
fold relative to control
3
2
1
H2aΔgly
H2aΔgly +shTusc3
d
Chase (h) 0 3 6
35
H2aΔgly
35
H2aΔgly +shTusc3
H2aΔgly remaining relative to pulse (%)
100
80
60
40
20
0
ctrl
+shTusc3
*
0
2
4
6
Chase (h)

875

Fig. 5

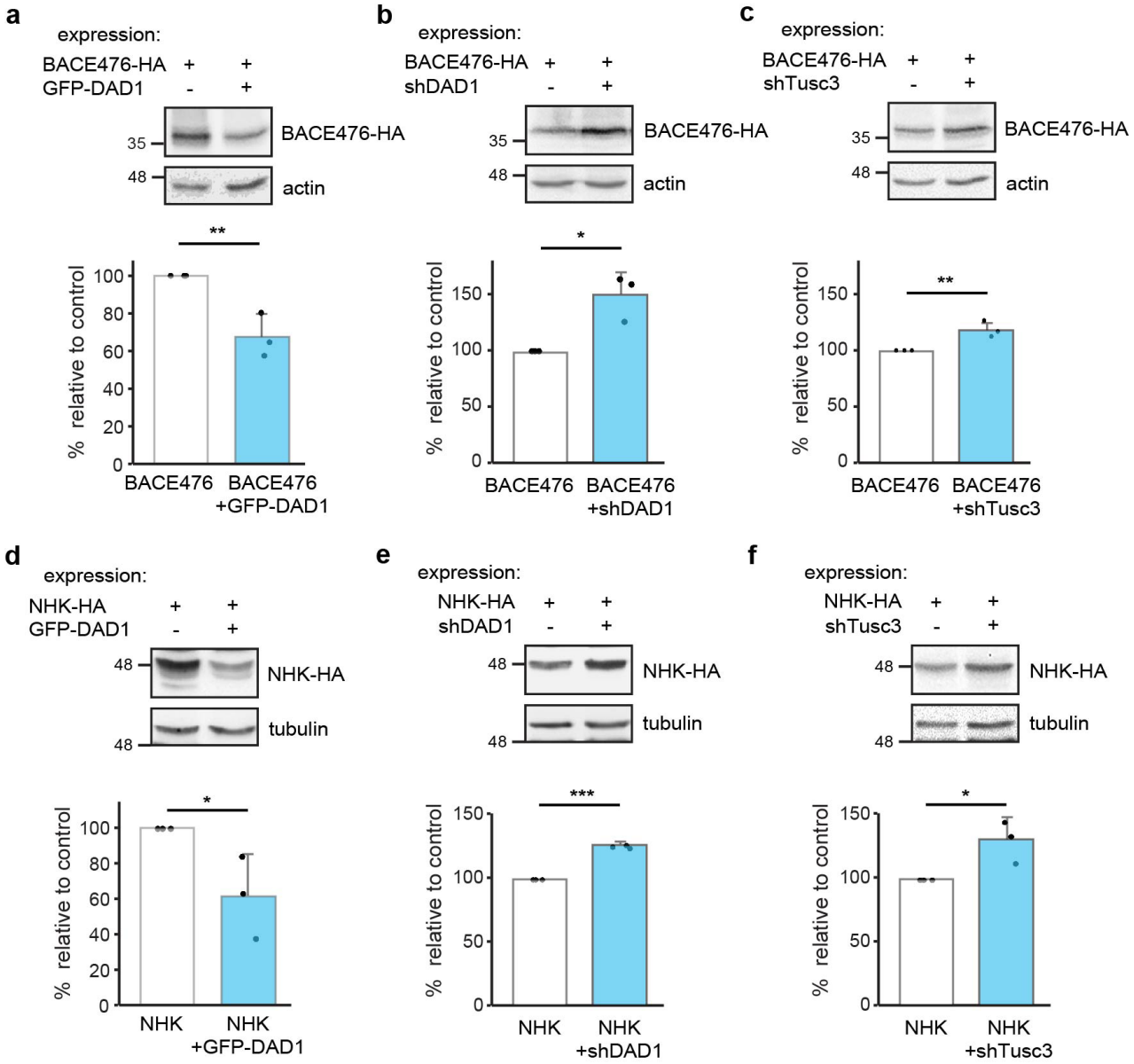
a
expression:
BACE476-HA + +
GFP-DAD1 - +
35
48
BACE476-HA
actin
**
% relative to control
100
80
60
40
20
0
BACE476
BACE476 +GFP-DAD1
b
expression:
BACE476-HA + +
shDAD1 - +
35
48
BACE476-HA
actin
*
% relative to control
150
100
50
0
BACE476
BACE476 +shDAD1
c
expression:
BACE476-HA + +
shTusc3 - +
35
48
BACE476-HA
actin
**
% relative to control
150
100
50
0
BACE476
BACE476 +shTusc3
d
expression:
NHK-HA + +
GFP-DAD1 - +
48
48
NHK-HA
tubulin
*
% relative to control
100
80
60
40
20
0
NHK
NHK +GFP-DAD1
e
expression:
NHK-HA + +
shDAD1 - +
48
48
NHK-HA
tubulin
***
% relative to control
150
100
50
0
NHK
NHK +shDAD1
f
expression:
NHK-HA + +
shTusc3 - +
48
48
NHK-HA
tubulin
*
% relative to control
150
100
50
0
NHK
NHK +shTusc3

878

Fig. 6

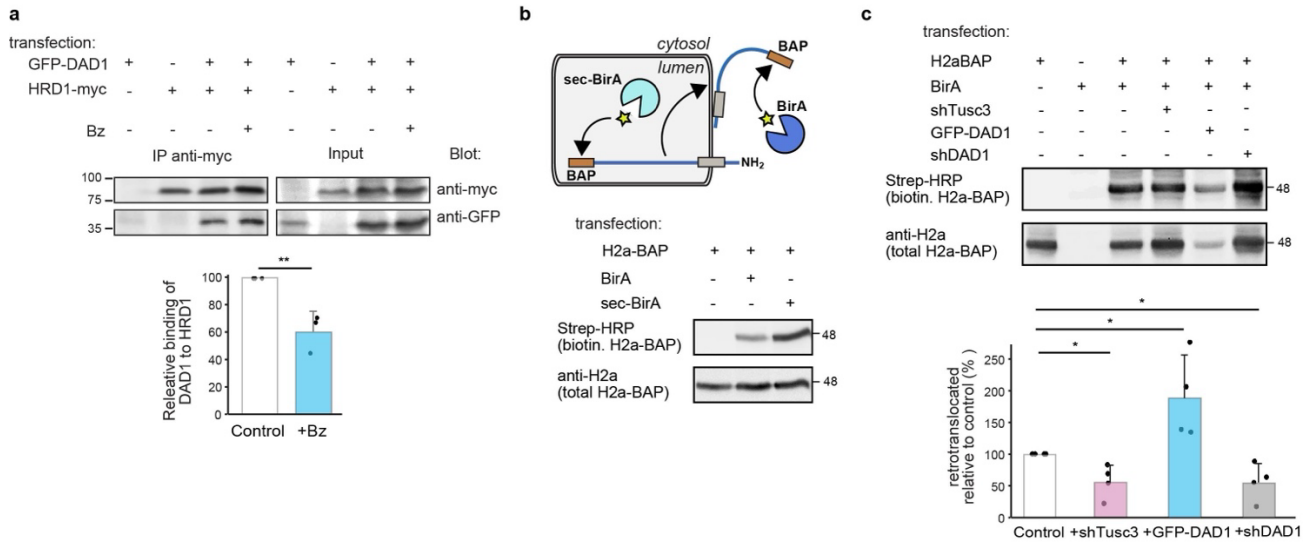

879

880

Fig. 7

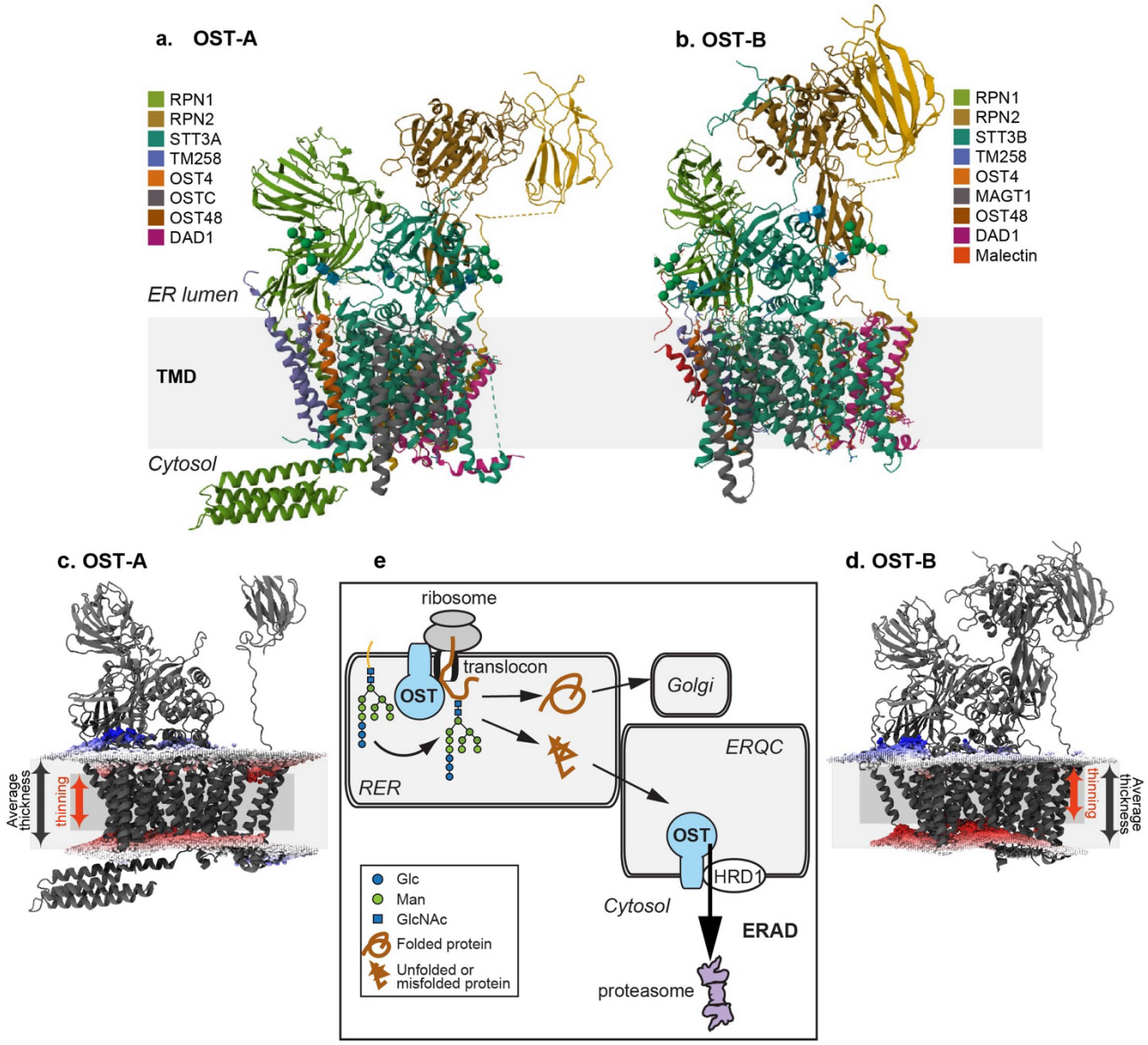
a. OST-A
RPN1
RPN2
STT3A
TM258
OST4
OSTC
OST48
DAD1
ER lumen
TMD
Cytosol
b. OST-B
RPN1
RPN2
STT3B
TM258
OST4
MAGT1
OST48
DAD1
Malectin
c. OST-A
Average thickness
thinning
d. OST-B
thinning
Average thickness
e
ribosome
translocon
OST
Golgi
ERQC
RER
OST
HRD1
Cytosol
ERAD
proteasome
Glc
Man
GlcNAc
Folded protein
Unfolded or misfolded protein

881